



**CHALMERS**  
UNIVERSITY OF TECHNOLOGY

---

# **The structure of metal-oxide interfaces investigated by genetic algorithms**

Master's thesis in Applied Physics

ALVARO POSADA BORBÓN

---

*Para mis papás,  
Alvaro y Dora Julia,  
con todo mi cariño.*

# The structure of metal-oxide interfaces investigated by genetic algorithms

ALVARO POSADA BORBÓN



**CHALMERS**  
UNIVERSITY OF TECHNOLOGY

Department of Physics  
*Division of Chemical Physics*  
CHALMERS UNIVERSITY OF TECHNOLOGY  
Gothenburg, Sweden 2016

The structure of metal-oxide interfaces investigated by genetic algorithms

© Alvaro Posada Borbón, 2016.

Supervisor: Maxime Van den Bossche, Department of Physics

Examiner: Henrik Grönbeck, Department of Physics

Thesis defense: June 3rd, 2016

Master's Thesis 2016

Department of Physics

Division of Chemical Physics

Chalmers University of Technology

SE-412 96 Gothenburg

Printed at Chalmers Reproservice  
Gothenburg, Sweden 2016

---

## Abstract

A global optimization study of oxide-supported metallic nanoparticles was carried out.  $\text{Cu}_{55}$  supported on  $\text{SiO}_2(0001)$ ,  $\text{TiO}_2(110)$  and  $\text{ZnO}(0001)$  substrates were used as model systems to investigate the preferred metal/oxide interface structure and conformation. The charge optimized many-body (COMB) potentials, coupled to genetic algorithm (GA) searches, were utilized to determine the structural motif of the supported nanoparticle. A second GA optimization was made to study the formation of mixed oxides between the particle and the support. Finally, the effect of oxygen vacancies and oxygen excess at the metal/oxide interface was investigated following the same framework as before. DFT re-optimization of the neutral  $\text{Cu}_{55}$ - $\text{ZnO}$  lower energy structures, for both the mixed and ideal interfaces, was performed.

Keywords: Global optimization, genetic algorithms, supported clusters, metal-oxides, interatomic potentials.

## Acknowledgements

I would like to thank the Mexican National Council on Science and Technology (CONACyT) and the Sonora State Government for the full scholarship that allowed me to carry out my Masters degree studies in Sweden. Scholarship reference number: 328617/383262.

I would like to thank my examiner and my supervisor Henrik Grönbeck and Maxime Van den Bossche, for their infinite patience, support and guidance throughout the duration of this project. I would like to make a special mention to Maxime, once again, for all the valuable discussions regarding global optimization problems, and for his invaluable help in the programming and scripting of the code.

I would like to thank all the people at Chemical Physics for creating such a nice work environment.

Finally, I would like to thank all the people I've met during my Masters studies at Chalmers, for the two wonderful years that have been.

Alvaro Posada Borbón, Gothenburg, June 2016

# Contents

<b>List of Figures</b>	<b>ix</b>
<b>List of Tables</b>	<b>x</b>
<b>1 Introduction</b>	<b>1</b>
1.1 Energy and environmental concerns . . . . .	1
1.2 Nanoscience and nanotechnology . . . . .	1
1.2.1 Catalysis . . . . .	2
1.2.2 Heterogeneous catalysis . . . . .	3
1.3 Theoretical and experimental background . . . . .	3
1.3.1 Experimental background . . . . .	4
1.3.2 Theoretical background and computational methods . . . . .	5
1.3.3 Choice of oxides . . . . .	6
1.4 Objectives of the thesis . . . . .	7
<b>2 Theory and Methodology</b>	<b>8</b>
2.1 Potential energy surfaces and the global minimum problem . . . . .	9
2.2 Evaluating the PES . . . . .	10
2.2.1 Interatomic interactions: An overview . . . . .	10
2.2.2 First Principle methods . . . . .	10
2.2.3 Interatomic Potentials . . . . .	11
2.2.4 Charge optimized many-body potential (COMB) . . . . .	13
2.3 Global minimum search algorithms as exploratory means of the PES . . . . .	16
2.3.1 Search algorithms: An overview . . . . .	17
2.3.2 Genetic algorithms . . . . .	17
2.4 Computational approach . . . . .	19
2.4.1 LAMMPS + ASE + CP2K . . . . .	19
2.4.1.1 Genetic Algorithm in this work . . . . .	19
<b>3 Results</b>	<b>21</b>
3.1 Bulk structures: SiO <sub>2</sub> , TiO <sub>2</sub> and ZnO . . . . .	21
3.2 Surface structures . . . . .	24
3.3 Gas Phase Clusters: Cu <sub>13</sub> , Cu <sub>38</sub> , Cu <sub>55</sub> . . . . .	26
3.3.1 Structural motifs and GA performance . . . . .	27
3.4 Supported nanoparticle . . . . .	30
3.4.1 Cu <sub>55</sub> -TiO <sub>2</sub> . . . . .	31

## Contents

---

3.4.2	Cu <sub>55</sub> -SiO <sub>2</sub> . . . . .	32
3.5	Cu <sub>55</sub> -ZnO . . . . .	33
3.5.1	Neutral ZnO . . . . .	33
3.5.2	Oxygen deficient ZnO - Cu <sub>55</sub> . . . . .	36
3.5.2.1	Ideal surface . . . . .	36
3.5.2.2	Mixed interface . . . . .	37
3.5.3	Oxidized ZnO - Cu <sub>55</sub> . . . . .	38
<b>4</b>	<b>Conclusions</b>	<b>39</b>
	<b>Bibliography</b>	<b>41</b>

# List of Figures

3.1	ZnO lattice parameter ( $a$ ) compared with first principles theoretical and experimental values found in the literature. . . . .	22
3.2	ZnO lattice parameter ( $c$ ) compared with first principles theoretical and experimental values found in the literature. . . . .	22
3.3	SiO <sub>2</sub> lattice parameter ( $a$ ) compared with first principles theoretical and experimental values found in the literature. . . . .	22
3.4	SiO <sub>2</sub> lattice parameter ( $c$ ) compared with first principles theoretical and experimental values found in the literature. . . . .	22
3.5	TiO <sub>2</sub> lattice parameter ( $a$ ) compared with first principles theoretical and experimental values found in the literature. . . . .	23
3.6	TiO <sub>2</sub> lattice parameter ( $c$ ) compared with first principles theoretical and experimental values found in the literature. . . . .	23
3.7	Titanium dioxide bulk structure. Shown as primitive cell . . . . .	23
3.8	Silicon Dioxide Bulk structure. Shown as a 2x2x2 cell. . . . .	23
3.9	Zinc oxide Bulk structure. Shown as a 2x2x2 cell. . . . .	23
3.10	The ZnO(0001) surface, showing both top and side view. . . . .	25
3.11	The SiO <sub>2</sub> (0001) surfaces, showing both top and side view. . . . .	25
3.12	The TiO <sub>2</sub> (110) surface, showing both top and side view. . . . .	25
3.13	Global minimum of Cu <sub>13</sub> obtained by the GA-Run . . . . .	27
3.14	The metastable Cu <sub>13</sub> structure, as obtained by the GA-run. . . . .	27
3.15	Frequency analysis of a set of GA runs for Cu <sub>13</sub> , using 10% mutation probability. . . . .	28
3.16	Cu <sub>38</sub> . Global minimum structure. . . . .	29
3.17	Cu <sub>55</sub> (Icosahedral motif). Global minimum structure. . . . .	30
3.18	Lowest energy Cu <sub>55</sub> structure on TiO <sub>2</sub> (110) with the COMB2A potential. . . . .	32
3.19	Lowest energy Cu <sub>55</sub> structure on TiO <sub>2</sub> (110) with the COMB3 potential. . . . .	32
3.20	GA optimized Cu <sub>55</sub> structure found on SiO <sub>2</sub> (0001) surface, using the COMB2A potential. . . . .	32
3.21	Schematic picture of carved surface. . . . .	33
3.22	Lowest energy Cu <sub>55</sub> structure supported on an ideal ZnO(0001) substrate. . . . .	34
3.23	GM Cu <sub>55</sub> supported on a mixed interface ZnO substrate. . . . .	34
3.24	Oxygen deficient ZnO-Cu <sub>55</sub> " <i>clustered</i> " vacancies structure (C1). . . . .	37
3.25	Oxygen deficient ZnO-Cu <sub>55</sub> " <i>diluted</i> " vacancies structure (C2). . . . .	37

3.26	Lowest energy $\text{Cu}_{55}$ structure on the oxygen deficient mixed interface support. . . . .	37
3.27	Lowest energy $\text{Cu}_{55}$ structure with oxygen excess on the mixed interface support. . . . .	38
3.28	Lowest energy $\text{Cu}_{55}$ structure with oxygen excess on the ideal interface support. . . . .	38

# List of Tables

3.1	Experimental and theoretical lattice parameters for all bulk oxides . . .	21
3.2	Lattice parameters for wurtzite ZnO as a function of system size. Obtained using COMB3 potential. . . . .	22
3.3	Lattice parameters for $\alpha$ – quartz SiO <sub>2</sub> as a function of system size. Obtained using COMB2A potential. . . . .	22
3.4	Lattice parameters for TiO <sub>2</sub> as a function of system size. Obtained from COMB2A relaxation. . . . .	22
3.5	Lattice parameters for TiO <sub>2</sub> as a function of system size. Obtained from COMB3 relaxation. . . . .	22
3.6	Surface energies for all oxide surfaces. . . . .	24
3.7	Energetical and structural comparison of Cu <sub>13</sub> clusters . . . . .	27
3.8	Frequency analysis of GA runs for Cu <sub>13</sub> with respect to mutation probability . . . . .	28
3.9	Absolute and relative energies for the Cu <sub>38</sub> cluster. . . . .	29
3.10	Energetic comparison of the GA-GM with the Cu <sub>55</sub> structures constructed using ASE. . . . .	30
3.11	Energetic differences of the lowest energy structure in the <i>ideal interface</i> vs. the <i>mixed interface</i> for neutral ZnO-Cu <sub>55</sub> . . . . .	35
3.12	Energies for stoichiometric (ideal) ZnO-Cu <sub>55</sub> from DFT calculations .	35
3.13	Energy for ZnO-Cu <sub>55</sub> mixed interface from DFT calculations . . . . .	35
3.14	Energy comparison for oxygen deficient ZnO-Cu <sub>55</sub> from the ideal putative GM. . . . .	36

# Introduction

## 1.1 Energy and environmental concerns

Ever since the world-wide energy crisis in the 1970's, which led to a deepened economic stagnation and a sudden increase in fossil fuels prices, efforts on research towards alternative and renewable energy sources have increased [1]. Joint to this obvious economic driving force lies now a more serious threat, namely climate change and resource depletion. It has gradually become apparent that we can no longer depend on a single non-renewable energy source that pollute and destroy our world. In the last couple of decades, these socio-economic affairs have sparked society's interest in sustainable means for energy production, environment remediation and preservation, and health related technologies. We are faced with problems that endanger our way and quality of living, and the scientific community has undertaken a noble endeavour facing these issues.

Despite this, fossil fuels are still the world's largest energy source [1]. However, science has come a long way since the seventies. Research in nanomaterials and surfaces sciences keep making promising advances in sustainable means for energy production. Fuel reformation, water splitting for hydrogen production, hydrogen storage and electro-and-photovoltaics are some of the current routes for a more sustainable future. It is in this area of research, on nanomaterials, on which I will try to contribute to with this thesis work.

## 1.2 Nanoscience and nanotechnology

We understand nanomaterials as materials where at least one of their spatial dimensions is in the order of magnitude of  $10^{-9}\text{m}$  [2]. Of special interest in the field of nanomaterials are nanoparticles (NPs), which are aggregates of zero-dimensional structures of sizes in the order of 1 to 20 nm [3].

It widely accepted by the scientific community that metallic nanostructured materials often exhibit a different set of physical and chemical properties in comparison to those of their larger counterparts, bulk-like materials [3–5]. These differences in characteristics can be explained, to some extent, by quantum effects introduced by the finite-size of the nanoparticles, under-coordination of atoms (number of nearest neighbours) and strain effects on the atomic lattice [5]. It is also known that nanoparticles exhibit a higher surface to volume ratio than bulk materials, since most of the atoms in the structure are present in the surface rather than in the bulk [5]. As it is mentioned by Mariscal et al. [4], it is precisely these differences in

physical and chemical properties from bulk material, joint to their high surface to volume ratio, that make nanomaterials so attractive.

The capability of designing cost-effective tailored materials has attracted, unsurprisingly, the attention of the scientific community. This has allowed for a wide variety of branches of science to merge into a very rich interdisciplinary field of research. Novel approaches have been developed in recent years concerning the subjects of catalysis, energy storage and production, photovoltaics, bio-fuel production, water cleansing, miniaturization of transistors, medical applications and drug delivery, only to name a few. This show us the profound impact research on this area has had, making it just as important as it is interesting.

Nanomaterials are of special interest in the field of catalysis, where they are used to minimize costs, due to their high surface/volume ratio. Furthermore, given the special reactivity and selectivity nanostructured materials show, they have become the workhorse for the chemical industry [6]. It is regarded that around 85-90% of the products made by the chemical industry are the result of catalytic processes [6, 7].

### 1.2.1 Catalysis

Catalysis is understood as a process where a substance, the catalyst, introduces a kinetically favourable reaction path, with a lower activation energy. This accelerates the rate of reaction in comparison to the uncatalyzed reaction, leaving the catalyst unaltered after the chemical interaction [8]. Importantly, catalysts only affect the kinetics of a reaction and not its thermodynamics, meaning that the overall change of free energy in the reacting system will be the same for both the catalytic and the non-catalytic reaction [6]. Catalysis was first recognized and defined as chemical phenomenon in the 19th century [9], but it was not until the early years of the 20th century that full in-depth systematic studies were carried in order to understand it [6, 8], where the invention of advanced spectroscopic techniques opened the flood-gates to the detailed study of surfaces reactions [6]. It is now known that reactivity and selectivity of a catalysts depends greatly on its shape and size and on the support/catalyst interaction [5].

We understand reactivity as the capability of the catalyst to chemically convert the reactants, while we understand selectivity of a catalyst as the ability of producing a desired chemical product. It is important to note that certain conditions must be satisfied in order to achieve high catalytic activity. Sabatier's principle, states that the interaction between the reactants and the catalyst must be "*just right*", neither too strong nor too weak [8].

A catalyst can be further categorized according to its state of aggregation compared to that of the reactants. On one hand, we refer to homogeneous catalysis when both the catalyst and the reactants are in the gas or liquid phase. On the other hand, we refer to heterogeneous catalysis when the catalyst is found in a solid phase, while the adsorbates are either in a gas or liquid phase. Furthermore, we have biocatalysis,

which specifically refer to enzymes [6,9]. In this project, we are mainly interested in studying materials for heterogeneous catalysis.

### 1.2.2 Heterogeneous catalysis

Heterogeneous catalysts often consists of chemically active metal clusters or nanoparticles dispersed on a porous oxide as a support material. In this way the surface area available is maximized for the catalytic reaction to take place, which has a direct impact on the catalytic activity [2]. Among these materials, late transition metals dispersed on porous oxide supports are the preferred choice for the chemical and automotive industry for both production and pollution control [10]. Also, they have become rather important in the development of fuel cells and photovoltaic cells, where their utilization is aimed both to generate alternative and renewable energies sources and to allow for efficient energy storage [10,11].

Research on supported metal nanoparticles is of the uttermost importance for this field. Proper detailed studies are needed on metal/support interactions in order to create materials for energy storage and conversion, and for the sustainable production of chemicals [11]. As it is expressed in the words of *de Jongh et al* (2013):

*"...if we are to rely on alternative energy sources (biomass, solar or nuclear) and avoid serious environmental problems, we must develop new and improved solid catalysts..."*

Nonetheless, research on the effect of the support on the structure and reactivity of nanoparticles has as of yet mainly assumed idealized interfaces.

## 1.3 Theoretical and experimental background

It is clear that comprehensive research is needed on the structural properties and metal-substrate interaction, if we want to fully develop cost-effective catalysts. In this endeavour, it is paramount to gain a deeper understanding of the effect of nanoparticle size and shape on reactivity and selectivity [5]. In pursuit of this goal, we have witnessed over the last fifty years the development of novel experimental, theoretical and computational approaches.

From the experimental side, the creation of spectroscopic and microscopy techniques, as scanning tunnelling microscopy and scanning force microscopy, coupled to precisely controlled deposition techniques, have allowed for precise characterization and study of supported nanoparticles. Alongside the advances made by experimentalists, different theoretical and computational approaches enable us to analyse these materials at the atomic (in some cases electronic) level. These approaches are based, to some extent at least, on the laws of quantum physics. Density functional theory, empirical potentials, embedded atom methods and glue potential based methods have been developed with the hope of predicting the structural motifs of these sys-

tems [12].

Theoretical and experimental approaches are both frequently used in the study of heterogeneous catalysts. However, despite both studying the same topic, the very nature of the approaches gives rise to two complementary ways of understanding catalysis and catalytic reactions. Theoreticians can provide some understanding on how interactions occur at the nanoscale, using detailed, but necessarily approximate methods, while experimentalist can observe, in a very real sense of the word, these interactions in real-life situations. Nonetheless, since the experimentally studied systems are so remote from ideal conditions, a detailed understanding on the origin of the phenomena witnessed can be hard to achieve [13]. It is clear that both sides can benefit from this collaboration.

Good theoretical modelling can help experimentalist by providing ideas on the structural motifs and chemical composition of nanomaterials. Additionally, it can also help by shading light on growth mechanism and structure-to-property relationships. Theoreticians themselves benefit from having ways to validate their results and by further understanding essential phenomena occurring in non-ideal situations.

In the following subsections, I will address in more detail both the theoretical and experimental background of research on heterogeneous catalysis.

### 1.3.1 Experimental background

Despite that experimental research on supported metallic NPs on oxide substrates has grown in an accelerated pace over the last couple of decades, there is still much that remains unknown. The number of publications that focus on detailed structural studies and local chemical composition of supported nanoclusters is limited [14]. This is mainly due to the highly complex experimental requirements to make local characterization studies on individual catalysts [15]. Regardless of this, experimentalist have acquired a great deal of expertise in controlled synthesis and design of nanomaterials [16].

Current methodologies, based on *bottom-up* or *top-down* approaches, allow for precisely controlled size, shape and chemical composition of nanomaterials, tailored for specific applications. We understand a *top-down* approach as one that creates complex nanostructures from bulk materials. Examples of these are lithography and etching methods [17]. The exact opposite is meant when we refer to *bottom-up* approaches, where the nanomaterials are grown, by self assembly, one atom (or molecule) at a time. These are usually wet chemical methods [17, 18]. Combination of these two types of approaches have allowed for self-assembled supported nanoparticles, with narrow size distributions, that show long range order [17, 19]. It has also become known that support materials may stabilize metallic clusters against sintering at high temperatures. Additionally, oxide substrates supports, are known to enhance both activity and selectivity of metallic NPs [16]. Detailed characterization and a well controlled synthesis of nanomaterials are paramount in order to properly

correlate the nanoparticle structure to its chemical properties [16].

One interesting experimental observation, for example, is the tendency for metal particles to oxidize at the interface with the support, with implications for both the particle's catalytic activity and sintering rate.

### 1.3.2 Theoretical background and computational methods

Theoretical approaches for the study of supported nanoparticles on oxide substrates are based, at different degrees, on quantum physics. The structural determination of the most stable geometry of a system can be done by either solving a system of Schrödinger-like equations, as in the case of density functional theory, Hartree-Fock and post-Hartree-Fock methodologies (*ab initio*) or by calculating interatomic interactions via atom-atom potentials. This is possible via mapping the potential energy surface (PES). Where the PES refers to the mathematical relation of the energy of an atomic system and its geometrical shape and atomic positions.

Out of the *ab initio* methodologies, DFT is the preferred electronic structure method for calculating ground state energies in computational chemistry. This is mainly due to its reasonable accuracy-to-computational-effort ratio [20]. Other quantum methods, like configuration interaction, Moller-Plesset, coupled cluster single-double and even regular Hartree-Fock are just too expensive for systems larger than just a couple of atoms. Coupled to the high cost of calculating ground state energies, comes the enormous effort it means to effectively map the systems PES. Even DFT becomes too expensive for the geometry optimization of systems involving more than a couple of tens of atoms [21].

Fortunately, simpler and cheaper theoretical methodologies have been developed for calculating atomic system energies. These are known as interatomic potentials (IPs) and are based only on nuclei coordinates and interactions. Where a mathematical function describes interatomic interactions of the system. The Gupta potential, embedded atom method (EAM) like-potentials, and the charge optimized many-body (COMB) potential are good examples of IPs whose parameters are fitted to *ab initio* calculations. The utilization of IPs reduces significantly the computational cost of making geometric optimizations of larger systems, although, this comes at the cost of reduced accuracy. It is important to note that IPs can also be fitted to experimental results.

Global Optimization algorithms are widely used for locating the PES global energy minimum. These are based on automatizing the mapping of the PES in smart ways, making it more cost-effective to search for the minimum energy structures [22]. Schemes like basin hopping, minima hopping and evolutionary algorithms have been greatly improved over the years. These mechanisms are based either on moving from one minimum to another, as in the case of minima-and-basin hopping, or on evolution strategies, as in the case of genetic algorithm.

Examples of DFT and/or interatomic potentials coupled to global optimization techniques can be found over the literature, although they are scarce. Some examples will be given on the next chapter. Additionally, very little research has been done on supported NPs at the nanoscale. Theoretical work has typically focused on gas-phase clusters and on individual ideal surface facets. Customarily, research on supported clusters focuses on sub-nanometric nanoparticles. This is mainly due to the high computational cost of searching through a higher-dimensional PES, coupled to the large intrinsic cost of simulating many hundreds of atoms [22].

### 1.3.3 Choice of oxides

When it comes to the theoretical modelling of supported clusters, the preferred surface studied found in literature is MgO (100 or 001) [23,24]. This is understandable since it is a very inert surface, given its high stability over a wide range of environmental conditions [23]. Joint to this apparent lack of diversity in substrate studies, the trending theoretical approach considers only an epitaxial interaction between cluster and substrate, without contemplating possible diffusion of cluster atoms into the surface and vice versa. This might be an oversimplified model for supported cluster interaction with oxide substrates. On top of this, for some supported nanoparticles, physical and chemical properties are sometimes strongly related to the actual nature of the support [25]. As a result, detailed studies are required to better understand the nature of many metal cluster/oxide support combinations.

In this project we have chosen three oxide substrates both of reducible and irreducible character. We define a reducible oxide as a material that shows at least two stable oxidation states [26]. These systems are used as models for a theoretical approach that does consider atomic self-diffusion between substrate and cluster. Given the scale of the systems we are interested on, at the nanoscale, we'll make use of the charged optimized many body (COMB) interatomic potentials. In choosing which metal-oxide combinations to study, we are constrained to the ones for which such COMB parametrizations exist. This leads to the choice of studying Cu nanoparticles supported on zinc oxide (ZnO), silicon dioxide (SiO<sub>2</sub>) and titanium dioxide (TiO<sub>2</sub>).

#### **Wurtzite zinc oxide (0001)**

Zinc oxide supported copper catalysts are known to be highly reactive and selective for the synthesis of methanol from CO or CO<sub>2</sub> [27–30]. Given the widespread use of methanol in the chemical industry, regarded as the third most important chemical in 2007 [29], and its use as main reacting agent for hydrogen production and utilization in methanol fuel cells, it is understandable that this system has been extensively studied. Despite this, a full understanding of the metal-to-substrate interactions is still lacking [GET REG HERE].

### **$\alpha$ -quartz silicon dioxide (0001)**

Silicon dioxide supported copper catalyst, similarly as ZnO, is widely utilized in the synthesis of methanol and hydrocarbon conversion for fuel cells [31]. This catalyst is also used in the hydrogenolysis of glycerol for the sustainable production of glycol-based chemicals [32]. The catalyst, functionalized with amine groups, has been successfully used for the efficient homocoupling reaction of terminal alkynes [33], which ultimately could be used for the design and construction of carbon scaffolds [34], organic conductors and supramolecular switches [35], applications that could have great positive impact in the design of materials for medical applications. Surprisingly, theoretical studies regarding global minimum structures of  $\text{Cu}_x$  supported on  $\text{SiO}_2$  are scarce.

### **Rutile titanium dioxide (110)**

Titanium dioxide has been one of the preferred materials in the field of photocatalysis, given its relative low band gap, several studies and novel approaches have been developed for its use in photovoltaic cells. Now a days, titania supported copper catalysts have come into utilization for CO oxidation [36], NO adsorption [37], water gas shift reaction [38] and methanol synthesis from  $\text{CO}_2$  [39]. Given its wide versatility, it is an interesting catalyst to further study.

## **1.4 Objectives of the thesis**

As described in the previous section, we have chosen three different metal-substrate systems to investigate interface interactions at the nanoscale, where we will focus on the structural properties of the interface in these systems. We have chosen to work with metallic Copper nanoparticles (55 atoms cluster), while the substrates comprises oxides of both reducible and non-reducible character, explicitly zinc oxide (ZnO), silicon dioxide ( $\text{SiO}_2$ ) and titanium dioxide ( $\text{TiO}_2$ ) respectively. In order to find the most stable structure, genetic algorithm searches are performed, making use of the COMB potentials. We are interested in understanding if the current approach for supported clusters is sufficiently valid, i.e, understanding under which circumstances one needs to consider diffusion between the cluster and the substrate, if any, shading some light on substrate-cluster surface interaction.

# Theory and Methodology

Currently there are various theoretical modeling tools available for research on supported nanoparticles. The choice of whether to make use of quantum-physical calculation methods, like DFT, or to use the cheaper interatomic potentials methods, coupled to mapping schemes of the PES, is strongly based on the system size and character of the studied problem [12].

On the one hand, quantum-mechanical approaches are based on solving a many-electron Schrödinger equation. This is possible thanks to the Born-Oppenheimer approximation, which lets us separate electronic contribution from nuclear contributions in the total Hamiltonian. In the specific case of density functional theory, the main concept is to express the total energy as a functional of the electronic density, which transforms a many-electron problem into many one-electron problems. On the other hand, interatomic potentials are based on the Born-Oppenheimer approximation as well, but are fitted functions that mimic *first principles* or experimental results. In this latter case the interatomic interactions are reproduced by mathematical functions dependent on interatomic distances. When faced with choosing the level of theory needed for an accurate description of the systems PES, one has to consider the nature of the bonds in the system. Although more accurate in the description of bonding nature, first principle calculations can be too costly when modeling "large" systems. If the bonding can be accurately enough described using interatomic potentials, these become the method of choice.

It is important to keep in mind that the structural and dynamical properties we find in molecular and atomic systems, are directly related to the underlying potential energy surface (PES) [40]. This can be easily understood when we consider the definition of a PES, which refers to the mathematical relation of the energy of an atomic system and its geometrical shape and atomic positions [41]. From this definition, it is fair to say that a detailed study of structural properties and surface interactions on supported cluster becomes a problem of efficiently mapping the PES, on the lookout for the lowest energy structures. This is, the geometrical optimization problem is then only a global optimization problem.

A systematic and smart mapping of the system's PES, that leads unequivocally to the lowest energy structure, can represent a tough and tortuous endeavour. Additionally, the calculated PES of the system must be faithful to the actual nature of the system itself.

In the following subsections of this chapter, the global optimization problem and its relation to our systems of interest will be discussed.

## 2.1 Potential energy surfaces and the global minimum problem

As it was presented in the introduction to this chapter, there is a direct mathematical and physical correlation between atomic positions and the total energy. This is the system's underlying potential energy surface (PES). This mathematical function is a  $3N$  dimensional object that lies in a  $3N+1$  dimensional space, where  $N$  is the number of atoms in the system [40]. Now, just for completeness, we must mention that the potential energy of a system, in the absence of external fields, is invariant to three rotational and three translational operations. This brings the dimensionality of the object to  $3N-6$ , this, for non-linear systems.

It is important to point out that a PES does not depend on temperature, whereas the *free energy surface* (FES) does depend on temperature. This can be quickly explained when one remembers that for the PES the energy is a function of atomic positions and potential interactions. This will temperature effect on the FES and PES will be further discussed when we review some methodologies for PES mapping.

The concept of PES finds its theoretical foundation in the Born-Oppenheimer approximation (BO). This approximation, widely used in computational modeling of atomic structures, considers the atomic nuclei to be so massive in comparison to the electrons, that they appear as stationary. It is straightforward to show from this approximation, that the systems molecular Hamiltonian can then be split into electronic and nuclear contributions. From this, it can be shown that the electronic ground state energy of the system can be considered a function of the nuclear coordinates [42]. This is, the electrons of the molecular system move in a field generated by the stationary nuclei, while, at the same time, the nuclei experience forces from the electronic motion [43]. After the Hamiltonian is separated in nuclear and electronic contributions, the set of electronic equations are solved iteratively, and the total energy of the system provides the PES for nuclear motion [43]. This means that the motion of the nuclei, for each electronic state, is determined by a single PES [40]. A detailed explanation of this can be found in Szabo and Ostlund's *Modern Quantum Chemistry* (1996).

It was elucidated a couple of decades ago that vital information about structural and dynamical properties of atomic systems could be obtained from carefully mapping the underlying PES [44]. As stated earlier in this chapter, we can infer then that a detailed study of structural and energetic properties of an atomic system, can be viewed as a problem of efficiently mapping the PES, on the lookout for the lowest energy structure. It is simple to see how a local minimum in the PES corresponds to metastable configurations, since at the minima, the forces have to be zero, as  $\mathcal{F} = -\nabla V(\mathbf{r})$  [40]. The quality of the PES depends on the faithful description of the interatomic interactions. Based on this idea, many methodologies, comprising the different levels of theory, have been created to evaluate and map the PES of atomic systems.

## 2.2 Evaluating the PES

### 2.2.1 Interatomic interactions: An overview

We have made it abundantly clear that the geometric configuration of a system's nuclei, fully determines the system's ground state electronic energy. This is true, as long as the BO approximation is applicable. From this, we can roughly separate the methodologies for evaluating the potential energy surface into two levels of theory. Those based on *first principle* calculations and those based on *force fields* (also known as *interatomic potentials*). The former kind of approaches rely on solving the electronic ground state structure problem, i.e, they constitute a quantum mechanical approach. The latter type of approaches are based on a somewhat more classical description of interatomic interaction, as it has been mentioned before.

Both levels of theory can be further subdivided into different categories, dependent on the approximations made by each specific approach to deal with problem of calculating the system's energy.

### 2.2.2 First Principle methods

From the side of *first principle* methodologies we can subdivide the approaches based on whether or not they are based on solving the system's electronic Schrödinger equations by means of wave functions (WF). This is the case for Hartree-Fock and post-Hartree-Fock methods. In the case of DFT, the system's electronic ground state is described in terms of the total electronic density [20]. A major advantage of density based methods compared to WF based methods is the better scaling of computational cost with increasing number of electrons. I will now devote some attention to DFT, since it is the only *first principles* methodology used in this work.

Density Functional theory is a self-consistent quantum mechanical formulation for the description of the ground state electronic structure. The main assumption behind this theory is that we can express the energy of a system as functional of the electronic density following Kohn-Sham formalism, all of this under the Born-Oppenheimer approximation. This allows for the decomposition of a intractable many-electron problem into a set of solvable non-interacting single-electron problems. It's not the purpose of this work to go into detail about DFT, so we encourage the reader to review the seminal work of Hohenberg and Kohn [45] and Kohn and Sham [46], where the original formulation of the theory is made.

Out of the many theoretical first principles methods, DFT offers a good trade-off between accuracy and computational effort, which makes it the "*golden boy*" of computational chemistry. Nevertheless, also DFT suffers from a rapid increase in computational effort as a function of system size, which hampers its applicability to larger systems. It is regarded that, when working on a global minimum search problem, DFT can be applied for small systems consisting of at most  $\sim 100$  atoms. Good examples of theoretical work based on DFT coupled to effective sampling of

the PES for gas-phase and supported clusters are the ones carried by Hammer [47], Johnston [48] and Barcaro [49], based on either genetic algorithm or basin hopping mapping of the PES.

### 2.2.3 Interatomic Potentials

Interatomic potentials (IP), as the name suggests, refers to mathematical models that are fitted to empirical or semi-empirical data in order to describe interatomic interactions in a given system. Classic cases of these are for example the pair potentials of Lennard-Jones (LJ) or the Morse potential, where interaction between particles are taken by pairs at a time. This is exemplified in the LJ potential in equation 2.1

$$U_{LJ}(r_{ij}) = 4\epsilon \left[ \left( \frac{\sigma}{r_{ij}} \right)^{12} - \left( \frac{\sigma}{r_{ij}} \right)^6 \right] \quad (2.1)$$

$r_{ij}$  refers to the interatomic distance between two atoms, while the parameters  $\sigma$  and  $\epsilon$  can be fitted to the material properties from either first principle calculations or experimental measurements. It is clear that this sort of potential would face serious limitations when working with e.g. supported clusters, but it has been successful in describing van der Waals-bonded systems such as noble gases [50].

Much more realistic potentials have been created to better describe interatomic interactions of metal and oxide nanomaterials, as in the case of the widely used Gupta potential, the embedded atom method (EAM), or charge optimized many-body potentials (COMB), which take into account many-body interactions and directionality of bonds. These potentials are based on many-body interactions, and the total energy is described as a sum of all of these interactions. This sort of potentials has a much affordable computational cost than full first principle calculations, while grasping fairly well the essence of metallic bonding, in the case of Gupta and EAM, and directionality and charge equilibration, in the case of COMB. They offer reasonable results on length and time scales mostly inaccessible for DFT calculations [51]. As interatomic potentials are often designed to describe only certain types of bonding, transferability can be limited [50].

Two significant developments have been made in recent years, that have improved the accuracy and transferability of interatomic potentials. These are the further development of the *bond order* concept and the implementation of automated charge equilibration. [50]. The *bond order* is a measurement that represents both the strength and type of local bonding state [50, 52]. Interatomic potentials that rely on the *bond order* parameter are known as reactive potentials. These reactive potentials are capable of reproducing the effect of different bonding states [50], which make them more robust when it comes to transferability.

The concept of *bond order* and its relation to the bonding energy has a sound theoretical foundation on quantum physics. This was first presented by Abell [53] in 1985. The basic idea behind his work is that the electronic contribution to the

bonding energy in a pairwise interaction is fully modulated by the bond order, which depends mostly on the number of nearest neighbors. [54]. This is known as the second moment approximation in the tight binding theory. In simple words, the bond order depends on the local environment, meaning that an atom with fewer neighbors creates stronger interatomic bonds than an atom with more neighbors [55]. A full derivation of this approximation goes beyond the scope of this thesis work, so we urge the reader to review the work of Abell [53] or the work by Brenner *The art and science of an analytic potential* (2000), where a simple but complete explanation is given. A direct consequence of building an analytic potential on the basis of the concept of *bond order*, is that the explicit electrostatic interactions are overlooked. This is addressed by introducing either fixed charged Coulomb interactions as an additional term of the potential or by utilizing a *dynamic charge scheme*. In this later case, the principle of electronegativity equalization is utilized to determine the geometry dependent charge equilibration in the system. This approach is followed in the COMB potential [50].

While working with global optimization of supported nanoparticles under  $\sim 200$  atoms, as is the case with our supported clusters, it is still feasible to make use of a coupled approach DFT+IP, joint to a smart mapping procedure of the PES. In this regime, it is possible to carry a systematic and thorough search over the PES initially with the IP, and subsequently making a local geometry re-optimization of the lowest energy families of structures with DFT. This allows for corroboration of the results obtained with the IP optimization and, if necessary, correction and possible re-parametrization of the potential [12]. This sort of approach has been implemented successfully in gas-phase and supported clusters by Mottet [56], Ferrando [57] and Johnston [48].

Using empirical potentials approaches becomes "*mandatory*" when the supported nanoparticle is over  $\sim 1000$  atoms [12]. At these length scales even doing a single geometry optimization with DFT is very costly and one has to rely completely on the accuracy of the IP. Luckily at this system size interatomic behaviour becomes more bulk-like, so, IP might be a good choice for a fair energetic and geometrical description of the structures. Of course there is no guarantee that the IP will be accurate enough to fairly describe the system interactions, just based on system size. It is good to keep in mind that although locating global minimum structures can be a complicated process, this is just a first, necessary but not sufficient, step for the research of more complex interactions and phenomena in more realistic environments for the field of heterogeneous catalysis and computational chemistry. In order to gain profound knowledge on shape-to-property relationships of supported catalysts, kinetic studies are needed to understand the formation mechanisms that rule structural behaviour [21].

After this general introduction to IPs, we will focus on the IP used in this work. In the following subsections, a description of the approach followed for this thesis is given.

### 2.2.4 Charge optimized many-body potential (COMB)

The charged optimized many-body potential (COMB) is an interatomic potential built upon the platform of an Abell-Tersoff potential. This refers to the potential being based on the *bond order* concept, while taking into account the directionality of bonds in the system. This is simply done by considering a three-body interaction in the *short range* term of the potential, that considers angular dependence of relative atomic positions. Coupled to this, COMB potentials make use of a dynamic charge equilibration, based on the principle of electronegativity equalization for the electrostatic interactions [50].

The charge equilibration is done by following the formalism of Rappè-Goddard [58], where the electrostatic potential energy is approximated as a Taylor expansion with respect to the charge. From the Mulliken definition of electronegativity, understood as the average of the sum of ionization potential and electron affinity, and considering interaction for a full molecular system, it is straightforward to show that the potential is a function of electronegativity and the Coulomb energy [42]. The equilibration is achieved by considering the derivative of the potential, which for all intents and purposes can be seen as an atomic chemical potential. In equilibrium, the chemical potentials (of charge A and charge B) are equal [59], so charges will naturally flow from low electronegativity sites to high electronegativity ones (reverse situation as of chemical potential) [42]. For the COMB potential, the Coulomb interaction is modeled by Coulomb charge density integrals [50]. A full derivation of this can be found in Rappè and Goddard’s paper *Charge Equilibration for Molecular Dynamics Simulations* or in Leach’s *Molecular Modelling*. Something that must be noted, is that both of these characteristics, the charge dynamic equilibration and the bond order concept, have solid basis on quantum physics theory, and is reviewed in [54,59].

The charge equilibration scheme and the transferability achieved by having a *reactive potential* make COMB attractive for this thesis work. In addition, the potentials have been previously parametrized to account for metal-oxide supported systems [60], which should assure some fidelity to the PES we have worked with.

The COMB potential was first created in 2007 and has ever since been optimized with the intention of improving transferability for many systems. The current version, COMB3, is considerably more robust than previous versions. This can be seen from the fact that the COMB3 potential depends on about 70 parameters, while the second version of the potential, COMB2010 (a.k.a COMB2B) depends only on about 45 parameters. The parameters are fitted to first principles DFT calculation on pure bulk systems and binary systems as well as on supported nanoparticles [61]

The potential, regardless of the changes it has gone through, keeps a general shape, which can be seen in equation (2.2)

$$\begin{aligned}
 U^{tot} [\{q\}, \{r\}] = & U^{es} [\{q\}, \{r\}] + U^{short} [\{q\}, \{r\}] + \dots \\
 & \dots + U^{vdW} [\{q\}, \{r\}] + U^{corr} [\{q\}, \{r\}]
 \end{aligned}
 \tag{2.2}$$

The first term ( $U^{\text{es}}$ ) corresponds to the systems electrostatic energy, the second one ( $U^{\text{short}}$ ) takes into account *short range* interactions (*bond order* term), the third one ( $U^{\text{vdW}}$ ) considers long range *van der Waals* interactions via a LJ potential and the fourth term ( $U^{\text{corr}}$ ) is a correction term [50]. From equation (2.2),  $q$  and  $r$  refers to charges and relative positions, respectively. I will only further explain the components of the short range and electrostatic terms, since they contain the *bond order* concept and the *charge equilibration* scheme.

In equation (2.2), the term for short range interactions ( $U^{\text{short}}$ ), can be explicitly written as:

$$\begin{aligned} U^{\text{short}}[\{q\}, \{r\}] &= \sum_i \sum_{j>i} V_{ij}^{\text{bond}} \\ &= \sum_i \sum_{j>i} \left\{ F_c(r_{ij}) \left[ V^{\text{R}}(r_{ij}, q_i, q_j) - \frac{b_{ij} + b_{ji}}{2} V^{\text{A}}(r_{ij}, q_i, q_j) \right] \right\} \end{aligned} \quad (2.3)$$

Where  $F_c$  is the Tersoff cutoff function [55],  $V^{\text{A}}$  is an exponentially decaying attractive term,  $V^{\text{R}}$  is an exponentially decaying repulsive term and  $b_{ij}$  and  $b_{ji}$  are the three-body *bond order* terms. We must note that generally  $b_{ij} \neq b_{ji}$ .

$V^{\text{A}}$  and  $V^{\text{R}}$  are given by, respectively,

$$V^{\text{R}}(q_i, q_j, r_{ij}) = A_{ij} \exp \left\{ -\lambda_{ij} r_{ij} + \frac{1}{2} [\lambda_{ii} D_i(q_i) + \lambda_{jj} D_j(q_j)] \right\} \quad (2.4)$$

and,

$$V^{\text{A}}(q_i, q_j, r_{ij}) = B_{ij} B_{ij}^* \exp \left\{ -\alpha_{ij} r_{ij} + \frac{1}{2} [\alpha_{ii} D_i(q_i) + \alpha_{jj} D_j(q_j)] \right\} \quad (2.5)$$

The bond order term are calculated as,

$$b_{ij} = \left[ 1 + \left( \beta_i \sum_{k \neq i, j}^{NN} F_c(r_{ik}) \xi_{ijk} g(\theta_{ijk}) \right)^{n_i} \right]^{-\frac{1}{2n_i}} \quad (2.6)$$

with

$$\begin{aligned} \xi_{ijk} &= \exp \left[ \alpha_{ij}^{m_i} (r_{ij} - r_{ik})^{m_i} \right] \\ g(\theta_{ijk}) &= 1 + \frac{c_i^2}{d_i^2} - \frac{c_i^2}{d_i^2 + (h_i - \cos\theta_{ijk})^2} \end{aligned} \quad (2.7)$$

The index  $i$  corresponds to the central atom and the index for  $j$  and  $k$  refer to the neighbor atoms.

Looking back at equation (2.2), the term for *electrostatic* interactions can be written as,

$$\begin{aligned}
 U^{es} [\{q\}, \{r\}] = & U^{self} [\{q\}, \{r\}] + U^{qq} [\{q\}, \{r\}] + \dots \\
 & \dots + U^{qZ} [\{q\}, \{r\}] + U^{polar} [\{q\}, \{r\}]
 \end{aligned}
 \tag{2.8}$$

The first term ( $U^{self}$ ) refers to the energy necessary to form a charge in the atom, which is directly related to the charge equilibration scheme. The second term ( $U^{qq}$ ) corresponds to charge-charge interactions, the third ( $U^{qZ}$ ) to charge-nuclei interactions and the fourth ( $U^{polar}$ ) to polar interactions [50]. I will further expand the first term, given its importance to the COMB formalism.

The  $U^{self}$  term is related to the energy necessary to create a charge on each atom [50]. This term can be conceptualized as the potential energy generated by an atom simple existence [42]. The atom's self energy is then expressed as a Taylor series expansion with respect to its charge,

$$U^{self} [\{q\}, \{r\}] = \sum_i V_i^A (q_i) = V_0 + \frac{\partial V}{\partial q_i} q_i + \frac{1}{2} \frac{\partial^2 V}{\partial q_i^2} q_i^2 + \dots
 \tag{2.9}$$

Considering the cases of both negatively charged and positively charged atoms, it can be very easily found that the first and second order terms of the expansion are related to the electronegativity ( $\chi_0$ ) and self-interaction Coulomb integral  $J_{ii}^0$ . With this idea in mind, the COMB potential considers the  $U^{self}$  as the Taylor expansion up to fourth order, as can be seen in equation (2.10)

$$U^{self} [\{q\}, \{r\}] = \chi_i q_i + J_i q_i^2 + K_i q_i^3 + L_i q_i^4
 \tag{2.10}$$

All other terms in the total potential (see eq. (2.2)), can be retrieved in the article by Sinnott (2013) *Classical atomistic simulations of surfaces and heterogeneous interfaces with the charge-optimized many body (COMB) potentials* [50].

I will finish this subsection on the COMB potentials by making simple review of the potential second and third versions, to point out the differences between them.

### COMB2010

The second version of the COMB potential (a.k.a COMB2) follows the general formalism presented before. However, some terms of the potential have changed, or are included, to allow for more transferability in the third version of the potential (COMB3). There are two subversion of COMB2, namely COMB2A (a.k.a COMB2010) and COMB2B (a.k.a COMB2011). It's quite unclear which version is the one available in the large-scale atomic/molecular massively parallel simulator (LAMMPS) code. Nevertheless, from a thorough literature search I figured out that Si-O interactions are parametrized under the COMB2A version in the LAMMPS software. This was done by direct comparison between the parameter file available on LAMMPS and the literature available on the specific parametrization for this material [62]. The conclusion drawn is that the potential versions available in LAMMPS

are COMB2A and COMB3. No article about the parametrization for Ti-O interactions under the COMB2 formalism was found, however this parametrization exists in the same potential COMB2 file in LAMMPS.

From equation (2.2), the potential keeps some of the general terms, while the only term that does not appear at all is the long range van der Waals interaction  $U^{\text{vdw}}$ . All other terms are included, although with some restrictions. The potential is then written as:

$$E_T = \sum_i \left[ E_i^{\text{self}} + \frac{1}{2} \sum_{i \neq j} V_{ij}(r_{ij}, q_i, q_j) + E_i^{\text{BB}} \right] \quad (2.11)$$

Comparing eq. (2.2) and eq. (2.11), we must note that  $E_i^{\text{self}}$  is only the first component from  $U^{\text{es}}$  (see eq.(2.8)) completely disregarding the contributions from  $U^{\text{qz}}$  and  $U^{\text{polar}}$ , while the rest remains the same. The second term in eq. (2.11) corresponds to the  $U^{\text{short}}$  in eq.(2.2) plus the self-interaction Coulomb integral found in  $U^{\text{qz}}$  from  $U^{\text{es}}$  [62].

### COMB3

The third version of the COMB potential is based in the 2011 version of COMB, while introducing some changes taken from the REBO2 potential to the short interaction term. This leads to a better description of organic materials [50]. This version of the potential is strongly based on the one extensively described before. In this work, COMB3 was used to describe the interactions in ZnO-based systems.

## 2.3 Global minimum search algorithms as exploratory means of the PES

Now we have covered in sufficient depth the concept of an empirical potential and have gone through the specifics of the potential chosen for this work. Now it is important to review how to sample the PES of a system. Sampling the PES is the action that allow us to search for the lowest energy structure (the global minimum (GM)). Looking for the lowest energy structure is based on the idea that this is the structure that we expect to find in nature [3], although this might not always be the case in real life situations. Kinetic limitings effects are usually present in reality, as metastable structures are far more common than not. On top of this, temperature effects can play some roll in making some PES local minimum competitive enough to make it relevant in experimental conditions. As it was discussed before, the PES is not temperature dependent, but the *FES* is. The free energy surface (FES) is conceptually similar to the PES, where actually the FES is the statistical average of the PES over most of the coordinates [63]. It is important to make this distinction since a very low laying minimum in the PES could just as well be not so far (energetically) from a local minimum in the FES. Temperature can "*flood*" low laying

minimums and can as well change barrier heights in the FES, effectively modifying the energy landscape around the GM structure, making the GM compete with local minimum structures.

### 2.3.1 Search algorithms: An overview

The problem of finding the lowest energy structure has been broadly studied and several techniques for sampling the PES have been developed. Techniques like simulated annealing, basin hopping and evolutionary algorithms are some of the most widely utilized to carry out this endeavour.

Simulated annealing (SA) is probably the first global optimization algorithm applicable to global structure optimization of atomic systems [40]. Its importance lies not only in being the first, but also in its simplicity and large transferability. The technique is based on the metropolis algorithm where the probability of accepting a new candidate is  $P(\Delta E) = e^{-\frac{\Delta E}{k_B T}}$ . In the words of Kirkpatrick himself, one of the creators of the technique, SA consists on melting the system of interest and slowly lowering the temperature until it no longer changes (it freezes) [64]. The obvious limitations with this method is that one can get stuck at metastable configurations, especially if the quenching is done too quickly.

Other methods for locating the global minimum depend on PES deformation, as in the case of the Basin Hopping (BH) method and the Minima Hopping method (MH). Basin hopping effectively transforms the PES by a local minimisation [40, 65]. The idea behind this algorithm can be view as a Monte Carlo search coupled with a local optimization for each step, where a metropolis acceptance criterion is applied [3, 40]. Accepting a step means that the energy of this structure is now the new putative GM. By doing this, the PES is transformed into a set of interconnected "steps", where the plateaus correspond the putative GM [40]. The advantage brought by this technique, although not obvious at first sight, its quite elegant. Since one has to move between these interconnected "steps", the step-size needed between Monte Carlo moves is significantly larger than for a regular Monte Carlo try [40]. It is somewhat ironic that the main idea behind the BH methodology can also be its main disadvantage. Since, if one gets stuck in a metastable configuration, there is little to no gain in using the BH algorithm [65].

If the reader is curious, an interesting discussion on other global optimization techniques can be found in Wales and Doye's "*Global Optimization by Basin-Hopping and the Lowest Energy Structures of Lennard-Jones Clusters Containing up to 110 Atoms*" (1997) [66].

### 2.3.2 Genetic algorithms

Evolutionary algorithms, as the name states, are a class of methods for global minimum optimization, that rely on Lamarkian biological evolution schemes [3, 40, 42]. These algorithms can be classified as genetic algorithm, evolutionary programming

and evolutionary strategies [42, 67]. Although there are some differences between them, I will focus only on the first one.

Genetic algorithms (GA) are based on the concept of natural evolution. This method adopts evolutionary operators like mating (crossover), mutations and generations, to explore the PES. The idea is that a population "mates" and "evolves" over a number of generations converging towards the most stable configuration [42]. Historically, a genetic algorithm is used to optimize "genes", which in this context would be atomic positions, encoded into a "chromosome". Each chromosome represents a trial solution to the problem [67]. Evolutionary operators are then applied to these chromosomes, until a stopping criteria is reached [3]. I mentioned earlier that the methodology is Lamarkian. This is the case since the characteristics that are passed over to next generation are acquired by the "parents" during their lifetime, rather than inherited [40].

GAs can be used for any kind of optimization, though it can be modified in order to better fit a specific problem [68]. I will describe a bit the specifics that lie behind GA optimization.

A GA works by first creating a randomly generated initial population. Each member of the population is ranked according to some "*fitness*" parameter, e.g. the total energy after local optimization. Then some candidates are selected from the population in a probabilistic way, according to their fitness, and are mated or mutated. The process of selecting the candidates is usually done by either a "*roulette wheel*" procedure or by "*tournament selection*" [67]. The roulette wheel method basically takes a candidate at "*random*" as soon as the fitness of the picked candidate is greater than a randomly generated number. The tournament selection on the other hand, takes a number of chromosomes at random from the population and the two candidates with the best fitness are selected as parents [67]. The act of mating the parents is known as *crossover*. The crossover procedure can be done in a variety of ways. The general approach is to select two parents and to cut them along a randomly chosen plane [67]. The combination of these two cut parents then forms the offspring [67]. The probabilities for choosing any of the available genetic operators are usually chosen before hand. Mutations are meant to modify a single candidate. Mutations generally used are *random displacements*, *random permutation*, *rattle* and *mirror mutation*, just to name some. The purpose behind mutation operations is to minimize the risk of population stagnation. This is, to introduce genetic diversity to the population [67].

Once the new candidate has gone through this process, its fitness is evaluated after local optimization. The last step on the GA algorithm determines which new candidates will make it to the updated population. This is usually based on the fitness of each candidate. Common practice is to always ensure only the best candidates makes it to the next generation. This is called "*elitism*" and it guarantees that the best candidate in a population won't get "*worse*" [67]. This whole process stops once the stopping criterion is reached. This criterion can be based on a certain number

of generations going by without finding another lower energy structure, or simply when the change in energy between subsequent best candidates reaches a threshold, or when the maximum number of iterations is reached.

A decent variety of GA codes can be found on the literature and online. While some of them are open source, others are in-house codes developed over many years. Some examples of these are the Birmingham Cluster genetic algorithm program (BC-GA) [67], USPEX [69], XTALOPT [70] and ASE-GA [47]. In this thesis work we have made use of the ASE-GA, which will be described in detail.

## 2.4 Computational approach

### 2.4.1 LAMMPS + ASE + CP2K

The scheme followed during this thesis work is based on an IP+DFT approach. First a GA search of minimum energy structure is performed for the supported cluster, where only the copper cluster is optimized (2000 steps). Secondly, a GA optimization of the interface atoms in the cluster and in the substrate was done (2000 steps). From this procedure, we produce two systems. One with no mixing between substrate-cluster atoms and a second system that does consider mixing between structures. This first two steps are done with the COMB potential. Finally a DFT reoptimization of the lowest energy structure is done for both systems. The DFT optimization is done with the CP2K software. Specifics about the parameters used for the calculations will be provided in the *Results* section.

#### 2.4.1.1 Genetic Algorithm in this work

Each GA search consisted of twenty runs. The initial population for each run consists of twenty randomly generated candidates. An elitist roulette wheel selection, as described in [67] is used for the mating selection. A cut-and-splice crossover, as described in [71], is applied. The mutation selected were: mirror mutation, rattle mutation and random permutation mutation (permutation only used for interface GA run). The overall mutation probability was selected to be 40%, while the mutations probability of selection were 50%-50% when only the mirror and rattle mutation were used. For the interface GA optimization the mutation probability of selection were 25%-25%-50% respectively for mirror, rattle and permutation mutation. The mirror mutation cuts the structure with a plane perpendicular to the surface in a random orientation, and subsequently mirrors the selected cutted structure. The rattle mutation assigns a probability to each atom with which it can be displaced. A displacement distance of 1.0 Å was found to be the optimal for the gas-phase clusters. This same conditions were utilized for the supported and mixed-interfaces GA. To avoid stagnation in the mixed-interface case, the permutation mutation was used. As the name states, this mutation chooses a number of atoms in the chromosome at random (with certain probability) and exchanges them with atoms of a different species in the same chromosome. More information about this mutations,

permutation and mirror mutation, can be found in the ASE webpage under the module of "Standardmutations" [72], or for the rattle mutation in [67].

The GA available in the Atomic Simulation Environment (ASE version 3.9.1), was used. To evaluate the system's energy, the COMB potential was used through the LAMMPS software. Version COMB2A was used for SiO<sub>2</sub> and TiO<sub>2</sub> and the version COMB3 for TiO<sub>2</sub> and ZnO. Local optimizations were done with either FIRE, MDMin, LBFGS or BFGS methods. This are specified in the results sections when needed.

The subsequent re-optimization of the found global minimum was done with the CP2K software using the PBE functional. The *Quickstep* method was used, with a *cutoff* energy of 200 Ry and a *Relative cutoff* energy of 30 Ry. Convergence criteria for energy optimization was set to  $10^{-6}$ Eh. A coupled pseudopotentials + LCAO approach was utilized. A double zeta basis set (DZVP-MOLOPT-SR-GHT) was used coupled with the potentials GTH-PBE-q11, GTH-PBE-q6 and GTH-PBE-q12 for treating the LCAO description of copper, oxygen and zinc, respectively.

# Results

In this chapter, I will describe the computational approach followed during this thesis work and the results obtained from it. I will present and discuss both structural and energetical aspects of the calculations carried. Given the nature of the COMB potential, which is fitted mostly to DFT calculations, the results will be compared mostly to first principles calculations. Some comparisons to experimental motifs observed will also be included.

## 3.1 Bulk structures: SiO<sub>2</sub>, TiO<sub>2</sub> and ZnO

Here I present the results obtained for the bulk structure calculations. These calculations were devised from the beginning as a convergence test for the COMB potential with respect to system size. Since the COMB potentials are mostly parametrized with respect to relatively large systems, a test on system size convergence was considered to be necessary. Three or more system sizes were chosen for each oxide. The selection of the size was done by trying to keep the ratio between the length of the  $\hat{x}$  and  $\hat{y}$  cell vectors close to unity. Lattice parameters are given for all sizes and are compared to both first principles calculations and experimental values for each system. Theoretical and experimental lattice values compiled from the existing literature can be found in Table 3.1.

<b>Bulk</b>	$a_{\text{Theo}}(\text{\AA})$	$c_{\text{Theo}}(\text{\AA})$	$a_{\text{exp}}(\text{\AA})$	$c_{\text{exp}}(\text{\AA})$
<b>ZnO</b>	3.284 [73]	5.290 [73]	3.249 [74]	5.204 [74]
<b>SiO<sub>2</sub></b>	4.890 [75]	5.490 [75]	4.916 [76]	5.405 [76]
<b>TiO<sub>2</sub></b>	4.545-4.641 [77]	2.919-2.966 [77]	4.580 [78]	2.950 [78]

Table 3.1: Experimental and theoretical lattice parameters for all bulk oxides

The system size convergence test results for ZnO and SiO<sub>2</sub> can be found in Tables 3.2 and 3.3. These results were compared against the first principles theoretical and experimental values found in Table 3.1. These are appreciated in Figures 3.1 and 3.2 for ZnO and Figures 3.3 and 3.4 for SiO<sub>2</sub>.

The relaxation of the structures was carried out by both optimizing atomic positions and cell volume and shape. These optimizations were made with the FIRE and MDMin local optimizers. The convergence criteria for the relaxation were  $10^{-4} eV/\text{\AA}^3$  for the largest stress component and  $10^{-2} eV/\text{\AA}$  for the largest force. Special care was taken for the TiO<sub>2</sub> system. Since its parametrization is available for both COMB2A and COMB3, we decided to relax it with both versions.

### 3. Results

ZnO	a(Å)	c(Å)
1x1x1	3.576	5.336
3x3x2	3.302	5.254
6x6x4	3.303	5.264

Table 3.2: Lattice parameters for wurtzite ZnO as a function of system size. Obtained using COMB3 potential.

SiO <sub>2</sub>	a(Å)	c(Å)
1x1x1	4.756	5.291
2x2x2	4.756	5.293
3x3x3	4.756	5.293

Table 3.3: Lattice parameters for  $\alpha$  – quartz SiO<sub>2</sub> as a function of system size. Obtained using COMB2A potential.

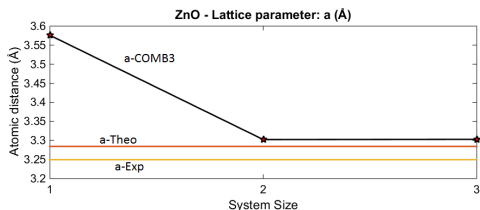


Figure 3.1: ZnO lattice parameter ( $a$ ) compared with first principles theoretical and experimental values found in the literature.

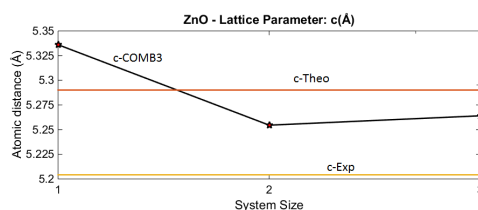


Figure 3.2: ZnO lattice parameter ( $c$ ) compared with first principles theoretical and experimental values found in the literature.

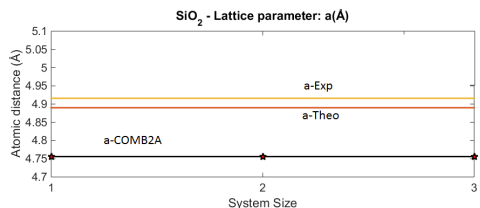


Figure 3.3: SiO<sub>2</sub> lattice parameter ( $a$ ) compared with first principles theoretical and experimental values found in the literature.

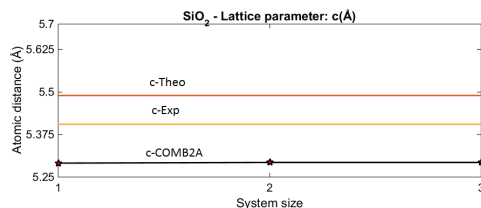


Figure 3.4: SiO<sub>2</sub> lattice parameter ( $c$ ) compared with first principles theoretical and experimental values found in the literature.

For the bulk structure of TiO<sub>2</sub> we found that both versions of the potential are equally good, when looking at large systems sizes. Results of this are presented next in Tables 3.4 and 3.5. As done for SiO<sub>2</sub> and ZnO, the graphical representation of this results compared to theoretical and experimental values are shown in Figures 3.5 and 3.6

TiO <sub>2</sub>	a(Å)	c(Å)
1x1x1	4.598	2.973
2x2x2	4.583	3.002
3x3x3	4.583	3.003
4x4x6	4.583	3.003

Table 3.4: Lattice parameters for TiO<sub>2</sub> as a function of system size. Obtained from COMB2A relaxation.

TiO <sub>2</sub>	a(Å)	c(Å)
1x1x1	4.588	3.259
2x2x2	4.542	2.962
3x3x3	4.562	2.967
4x4x6	4.565	2.967

Table 3.5: Lattice parameters for TiO<sub>2</sub> as a function of system size. Obtained from COMB3 relaxation.

### 3. Results

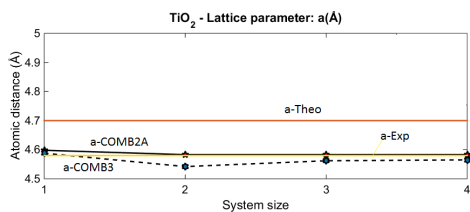


Figure 3.5: TiO<sub>2</sub> lattice parameter (*a*) compared with first principles theoretical and experimental values found in the literature.

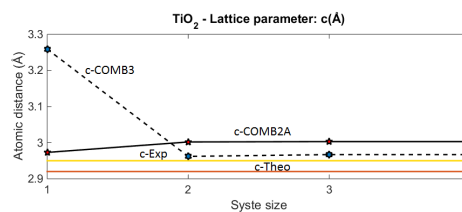


Figure 3.6: TiO<sub>2</sub> lattice parameter (*c*) compared with first principles theoretical and experimental values found in the literature.

As we can see from Tables 3.2 to 3.5 compared to the results available in Table 3.1, there is a clear trend for COMB3 to deviate from the desired structure when working with the (1x1x1) cell. Also, there is a clear tendency for lattice parameters to converge towards a certain value. Despite this, the overall results for the larger cells are in good agreement both with theoretical and experimental values found in the literature.

The reasons for the poor behaviour shown by the ZnO and TiO<sub>2</sub> (1x1x1) compounds has been speculated to be related to the long range term of the potential, which is probably overly dominant in this structures. The best structural motifs for each compound are shown in Figures 3.7, 3.8 and 3.9.

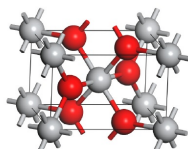


Figure 3.7: Titanium dioxide bulk structure. Shown as primitive cell

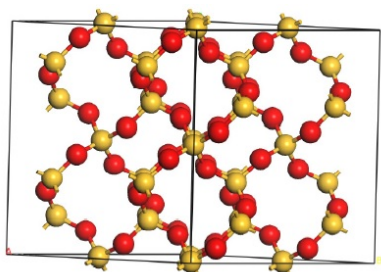


Figure 3.8: Silicon Dioxide Bulk structure. Shown as a 2x2x2 cell.

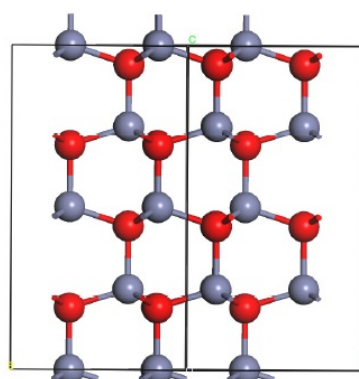


Figure 3.9: Zinc oxide Bulk structure. Shown as a 2x2x2 cell.

### 3.2 Surface structures

The following step in the project entailed cleaving the desired surfaces from each crystal structure. Specifically, the (110) plane for TiO<sub>2</sub>, and the (0001) plane for both ZnO and SiO<sub>2</sub>. All surfaces were cleaved from the bulk structure that best resembled the lattice parameters and had the lowest value for remnant stress and forces. This is the 1x1x1 for TiO<sub>2</sub> COMB2A, the 3x3x3 for SiO<sub>2</sub> and the 3x3x2 for ZnO. After cleavage, the surfaces were extended to an approximate length of  $\sim 25$  Å for both  $\hat{x}$  and  $\hat{y}$  cell vectors. This length was chosen so the cluster could be easily placed on the surface, avoiding, beforehand, spurious interactions between the periodically repeated images. Five-layered surfaces were created, to avoid having too thin slabs. This effectively gives relatively large surfaces, where ZnO is comprised of 640 atoms, SiO<sub>2</sub> of 540 atoms and TiO<sub>2</sub> of 960 atoms. The relaxations for this systems were done by keeping a fixed cell volume, i.e, only atomic positions were relaxed, since the correct lattice distances were already accounted for in the previous bulk system relaxations. Optimizations were done with the FIRE and BFGS local optimizers, with a criterion for convergence based on forces. The force criteria for convergence was chosen as  $F_{\max} \leq 10^{-3}$  eV/Å.

Surface energies were calculated and are compared to existing first principles and experimental results found in the literature. Surface energy is defined as,

$$E_{\text{surface}} = \frac{E_{\text{slab}} - E_{\text{Bulk}} \left( \frac{N_{\text{slab}}}{N_{\text{Bulk}}} \right)}{2A_{\text{slab}}} \quad (3.1)$$

$E_{\text{slab}}$  is the total energy of the slab,  $N_{\text{slab}}$  is the number of atoms in the slab,  $E_{\text{bulk}}$  is total energy of the bulk system,  $N_{\text{bulk}}$  is the number of atoms in the bulk structure and A is the surface area of the slab. We can see from this equation that the surface energy is the cost of energy to cleave the bulk system with the same composition. These results can be seen in the following Table (Table 3.6):

Surface	$E_{\text{surf}} \left( \frac{\text{eV}}{\text{Å}^2} \right)$	$E_{\text{surf}}^{\text{theo}} \left( \frac{\text{eV}}{\text{Å}^2} \right)$
ZnO (0001)	0.089	0.071 [79]
SiO2 (0001)	0.174	0.137 - 0.150 [80]
TiO <sub>2</sub> (110) COMB2A	0.032	0.029 - 0.116 [81,82]
TiO <sub>2</sub> (110)- COMB3	2.041	0.029 - 0.116 [81,82]

Table 3.6: Surface energies for all oxide surfaces.

Two immediate conclusions can be drawn from the bulk and surface relaxation results. The first one and most striking, is that results for the TiO<sub>2</sub>-COMB3 system should be taken with a pinch of salt. This, however, does not mean that all calculations for TiO<sub>2</sub> with COMB3 are unreliable, but one must be careful with this specific system. This result is far from what has been reported previously for COMB3 on the same titania surface [83], where the authors parametrize the potential for titania and obtain a surface energy of 0.088 eV/Å<sup>2</sup> [83]. The second immediate conclusion

is that ZnO parametrization in COMB3 is rather good.

The resulting surfaces can be seen in the following figures:

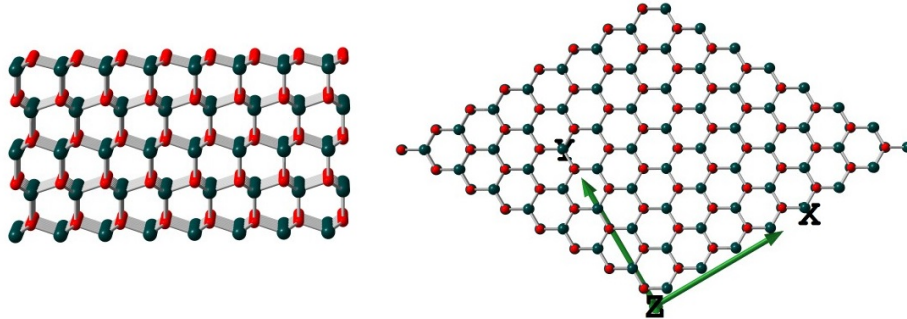


Figure 3.10: The ZnO(0001) surface, showing both top and side view.

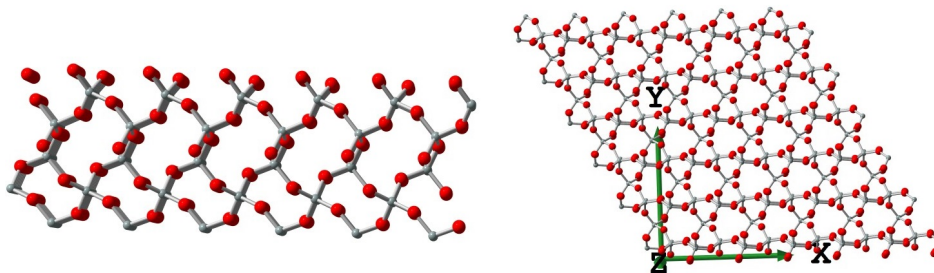


Figure 3.11: The SiO<sub>2</sub>(0001) surfaces, showing both top and side view.

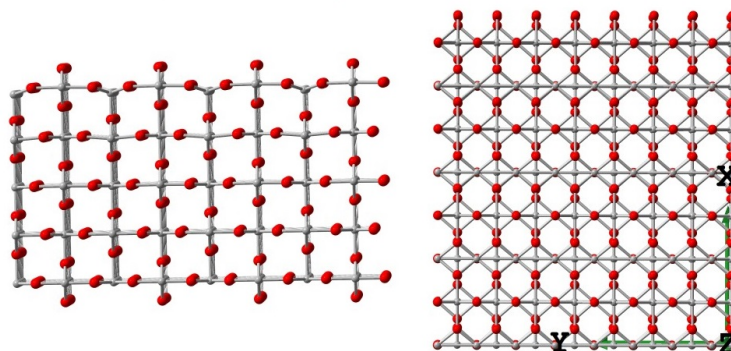


Figure 3.12: The TiO<sub>2</sub>(110) surface, showing both top and side view.

### 3.3 Gas Phase Clusters: $\text{Cu}_{13}$ , $\text{Cu}_{38}$ , $\text{Cu}_{55}$

Before going straight into the supported clusters, we decided to test the GA implementation coupled to the COMB potential by investigating the gas phase clusters. Three copper cluster sizes were selected, namely,  $\text{Cu}_{13}$ ,  $\text{Cu}_{38}$  and  $\text{Cu}_{55}$ . The size selection was not made at random. These were chosen to test both the COMB potential as to test the GA code. The thirteen atom cluster was chosen to test the fidelity of the potential. Given its small size, explicit quantum effects may influence the system's structure.  $\text{Cu}_{13}$  is known to show an icosahedral structure [84]. The 38 atom cluster was chosen because it has been studied before, and is known to adopt a truncated octahedral shape [66, 84]. This diversity of shapes was decided to be a good test for the GA. Finally, the 55 atom gas phase cluster was selected as a final test for both the GA and the potential. This result is important since the particle of interest for the supported nanoparticle is  $\text{Cu}_{55}$ . This last cluster size is known to have an icosahedral structure, with an inner shell of 13 and an outer shell of 42 atoms [48, 84, 85].

To make a fair energetic comparison of the GA structures, the global minimum (GM) obtained were compared to their pristine structures. The known structural cluster motifs were made with the octahedron and icosahedron libraries on ASE and relaxed with the BFGS local optimizer using the COMB2A potential. Comparison of results will be made in the following subsection.

As for the GA optimizations, the approach described in the *Computational approach* subsection in the *Theory and Methodology* section is followed. Each GA search consisted of twenty runs, with each run consisting of a population of twenty randomly generated candidates. As described before, an elitist roulette wheel method for candidate selection is used. The procedure is as described in Deaven and Ho's "*Molecular Geometry Optimization with a Genetic Algorithm*". Two parents are chosen with a certain probability and a randomly oriented plane cuts the parents by their center of mass. These two halves are brought together to form the offspring. If the number of atoms in the offspring is wrong, the cutting plane is translated in the normal opposite direction, until the right number of atoms is achieved in the offspring [86]. A mutation probability of 10% was found to be the optimal for the gas phase cluster optimizations made in this work. Since it makes no sense to randomly permute atoms in a homo-atomic cluster, only the mirror and rattle mutations were applied for these searches. A 50-50 probability of selection was assigned to each mutation. The optimal rattle strength parameter was found to be dependent on the number of atoms in the cluster. A statistical analysis was carried with the  $\text{Cu}_{13}$  cluster size. In order to obtain reliable statistical results, the number of runs used was increased from twenty to one hundred.

### 3.3.1 Structural motifs and GA performance

#### Cu<sub>13</sub> - cluster

The copper thirteen icosahedral structure was unequivocally found to be the global minimum. Remarkably, a metastable structure was found to differ from the GM by only  $\sim 3$  meV. The found global minimum and the metastable structure can be seen in Figures 3.13 and 3.14.

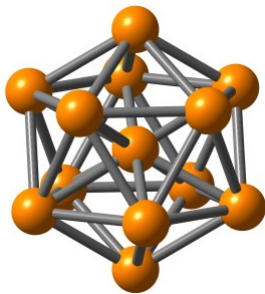


Figure 3.13: Global minimum of Cu<sub>13</sub> obtained by the GA-Run

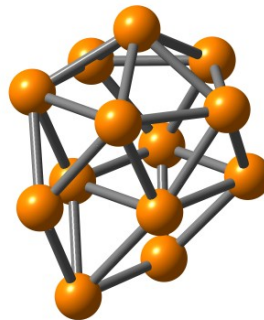


Figure 3.14: The metastable Cu<sub>13</sub> structure, as obtained by the GA-run.

The energetical comparison between the two structures found in the GA, and the optimized from ASE library can be found in Table 3.7. The energy of the GA-GM structure is used as a reference for the comparison with the other ASE-made icosahedral, octahedral structures and the metastable structure found in the global optimization. The distances between Cu-Cu atoms are presented. We make the distinction between *internal* and *external* distances, where the former refers to the average distance measured from the central atom to the other atoms, and the later refers to Cu-Cu average distance between the "*shell*" atoms in the cluster.

Cu <sub>13</sub>	GA-GM	Metastable	Octahedral
E <sub>tot</sub> (eV)	-29.416	-29.412	-29.076
E <sub>relative</sub> (eV)	0	0.004	0.340
Cu - Cu <sup>external</sup> (Å)	2.441	—	—
Cu - Cu <sup>internal</sup> (Å)	2.322	—	—

Table 3.7: Energetical and structural comparison of Cu<sub>13</sub> clusters

The frequency analysis, to determine how well the GA code performed, was carried out for different mutation probabilities. The optimal mutation probability was found to be 10%, this is shown in Table 3.8. The full analysis for the 10% mutation probability is now shown in Figure 3.15 (Hartke plot).

We can clearly see from Figure 3.15 that the GA is reasonably good, given that we find the GM known structure 12% of the times (success percentage of 12%). This can be observed from the histogram shown in the figure. A good way to quantify

% Mut	Half-life	Succes %	Av. # of Steps
<b>10</b>	10.335	12	458.08
<b>20</b>	11.790	7	331.57
<b>30</b>	12.053	7	600.14
<b>40</b>	11.294	6	505.00
<b>50</b>	13.293	11	576.64
<b>60</b>	13.881	5	428.40
<b>90</b>	9.610	2	575.50

Table 3.8: Frequency analysis of GA runs for  $\text{Cu}_{13}$  with respect to mutation probability

how efficient the GA algorithm is (mating and mutation), is to look at the "fitted half-life ( $\mathbf{X}$ )" parameter. The half-life tells us how many iterations are needed for the energy to decrease half of the value between that of a locally optimized structure and that of the GM [70]. The value obtained here for the half-life parameter  $\mathbf{X}$  of 10.335 is acceptable. The "Best-best" and "Worst-best" curves in the Hartke plot show us graphically how the energy optimization evolves per iteration for respectively the best and worst GA runs.

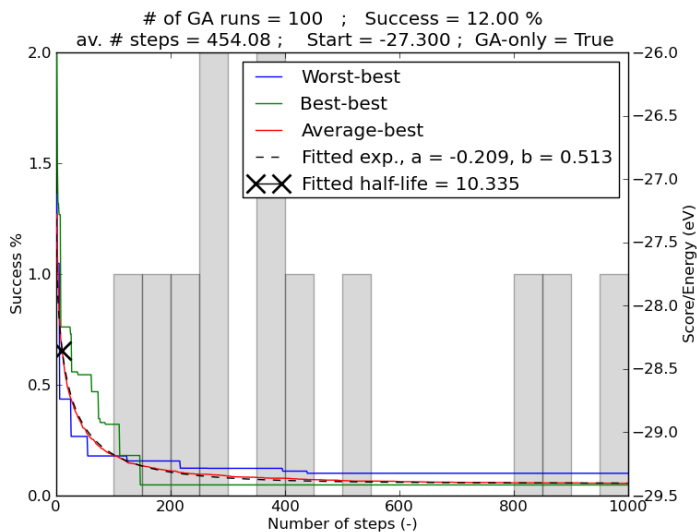


Figure 3.15: Frequency analysis of a set of GA runs for  $\text{Cu}_{13}$ , using 10% mutation probability.

### $\text{Cu}_{38}$ - cluster

The  $\text{Cu}_{38}$  structure found with the GA code was a truncated octahedron. This is in agreement with previous reported results for this system size [84]. In order to find this structure, the rattle strength was changed from displacements of 1.0 Å for the smaller size, to 1.3 Å for  $\text{Cu}_{38}$ . Since the structures are significantly different,  $\text{Cu}_{13}$  is an icosahedron while  $\text{Cu}_{38}$  is a truncated octahedron, the necessity to

change the value of rattle strength is understandable. As previously stated, the search consisted of twenty runs, with twenty candidates per run. For this structure size, we found the known GM structure in only one of the runs. This, however, is not statistically significant. The number of runs is not large enough to draw hard conclusions on the *goodness* of the GA for larger particles. It is possible to speculate that the success percentage will be less than for  $\text{Cu}_{13}$ , based only on the increase of dimensionality of the PES. However, further studies are needed to make a clear statement on that regard. All other parameters were kept the same as before. The number of iterations needed to find the known GM increased to 2500 iterations.

An energetic comparison is made for the GM structure found, as can be seen in Table 3.9. No special metastable structure was found. The obtained structure can be seen next in Figure 3.16.

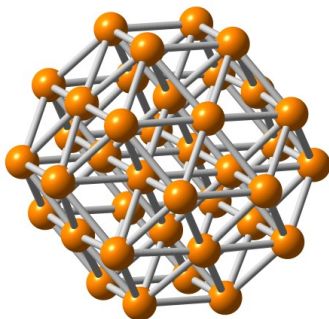


Figure 3.16:  $\text{Cu}_{38}$ . Global minimum structure.

$\text{Cu}_{38}$	GA-GM
$E_{\text{tot}}$ (eV)	-100.131
$E_{\text{relative}}$ (eV)	0

Table 3.9: Absolute and relative energies for the  $\text{Cu}_{38}$  cluster.

### $\text{Cu}_{55}$ - cluster

The  $\text{Cu}_{55}$  cluster was rather straight forward to search. The GM structure was found to be an icosahedral cluster. This is in agreement with previous studies [48, 84]. The same approach as for previous sizes was followed. Twenty runs were carried each consisting of twenty candidates, where the mutations used were the rattle and mirror mutations. A systematic testing for rattle strength values was conducted. Interestingly, the same combination of parameters (displacements of 1.0 Å with a probability of displacement of 40%) used for  $\text{Cu}_{13}$  (icosahedron) was the only one that successfully gave the proper conditions to effectively map the PES and locate the "known" GM. Once again, the number of iterations necessary to find the GM increased. This time 3700 iterations were needed.

The structural conformation of this cluster can be seen in Figure 3.17. As done for the previous clusters, the energetic comparison between the found structure and the octahedral structures from ASE libraries can be found in Table 3.10

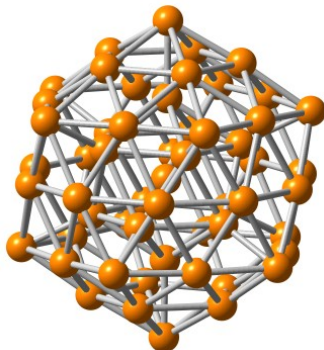


Figure 3.17:  $\text{Cu}_{55}$  (Icosahedral motif). Global minimum structure.

$\text{Cu}_{55}$	GA-GM	Octahedron ASE
$E_{\text{tot}}$ (eV)	-151.386	-148.394
$E_{\text{relative}}$ (eV)	0	2.991

Table 3.10: Energetic comparison of the GA-GM with the  $\text{Cu}_{55}$  structures constructed using ASE.

A significant difference in energy can be observed in Table 3.10 between the found GA-GM and the octahedron structure from ASE. This energetic difference is in good agreement with the results found in the literature, where the GM structure for  $\text{Cu}_{55}$  is found to be the icosahedral structure [48, 84].

### 3.4 Supported nanoparticle

For this final and most important part of the project, several changes were made to the GA code, although the working principles remained the same. It must be mentioned that the adaptation of the GA code for supported clusters and interface interactions was a challenge on its own. Parallelization of the code turned out to be more arduous than expected. Joint to this, enforcing the periodic boundary conditions (PBC) in the calculations showed us that there are some communication issues between the python interface implemented with ASE and the computing being done with the LAMMPS software. We eventually succeeded in properly parallelizing the code and correctly enforcing the PBCs.

The relaxed surfaces shown before in this chapter were utilized to work as a support for a GA optimized  $\text{Cu}_{55}$  cluster. As a first step to study interaction at the interface for this metal-oxide system a GA search was firstly done only on the pure  $\text{Cu}_{55}$  particle. The working principle of this search is the same as for gas phase structures. Of course, a major difference is that there is an energetic contribution and interaction

between the GA optimized copper atoms and the oxide substrates. To simplify the study, all the atoms in the substrate were constrained during the Cu<sub>55</sub> evolutionary optimization. A mutation probability of 10% was utilized, and only the mirror and rattle mutations were used. The mirror mutation was modified to allow only for perpendicular cutting planes with respect to the surface to be implemented. This was done to allow the GA to sample the PES on the lookout for an icosahedron-like supported structure, where the bottom atoms in the nanoparticle are stacked in a layer fashion with respect to the surface. Granting some "wetting" of copper atoms on the substrate. The parameters found to be effective for Cu<sub>55</sub> gas phase rattle mutation were used for this supported clusters.

In this study, the individual GA searches were terminated after two thousand iterations in order to limit the computation time. It can therefore not be guaranteed that the lowest-energy structures obtained are the true global minima. Considering the typical convergence behaviour of the GA, however, the energetical and structural differences with respect to the true GM are likely to be small. Furthermore, in practice also structures with energies slightly higher than the GM are relevant, due to the thermal energy ( $k_B T$ ).

The results of these GA searches are presented as follows.

### 3.4.1 Cu<sub>55</sub>-TiO<sub>2</sub>

The optimization of the Cu<sub>55</sub> cluster on TiO<sub>2</sub>(110) was done as mentioned before. Twenty runs, each with a population of twenty randomly generated initial candidates, were carried using the methodology described in Chapter 2, considering the modifications mentioned in the previous subsection. Regardless of the results previously obtained for COMB3 parametrization, the calculations were made with both COMB2A and COMB3 versions.

No cluster formation was observed on this surface, regardless of the potential versions utilized. For both COMB2A and COMB3, the lowest energy structure found with the GA searches was a monolayer of copper atoms over the titanium dioxide substrate. Cluster sintering and growth, is, however, known to occur in this type of oxide. We can only assume then that the COMB parametrizations are not reliable for our specific purposes. Also, the creation of a monolayer of copper atoms over the substrate hinders us on further studying interface interactions. It can be argued that introducing defects and/or vacancies into this surface might induce the formation of real cluster structures. Since similar effects have been observed for F-centers on the MgO(100) surface [87]. This might be a valid hypothesis, however, I have the feeling that this will not be enough to balance out the effects of the parametrization. A better alternative would be to re-parametrize the potential focusing on this unique system. I believe that a better parametrization of the potential can be achieved by including systems like nanometric supported nanoparticles to the fitting procedure of the COMB parameters. Ultimately, there is a need for full DFT calculations. The results obtained can be observed in Figures 3.18 and 3.19.

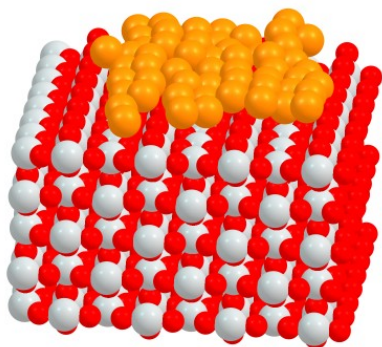


Figure 3.18: Lowest energy  $\text{Cu}_{55}$  structure on  $\text{TiO}_2(110)$  with the COMB2A potential.

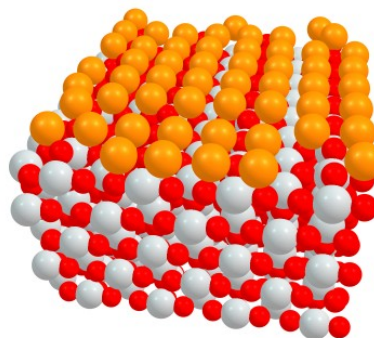


Figure 3.19: Lowest energy  $\text{Cu}_{55}$  structure on  $\text{TiO}_2(110)$  with the COMB3 potential.

### 3.4.2 $\text{Cu}_{55}\text{-SiO}_2$

The same procedure as for  $\text{TiO}_2$  was followed for  $\text{SiO}_2(0001)$ , with the only difference that Si-O-Cu interactions are included only in COMB2A. Interestingly, similar results as for titanium dioxide were obtained, although not as extreme. The lowest energy structure found through the GA search for the copper cluster showed that this prefers to wet the surface, while showing some conglomeration into a full standing cluster. It is hard still to see any kind of symmetry in the supported  $\text{Cu}_{55}$ , which might mean that the structure is still far away from the GM. Further mapping of the PES should be done before trying to study interface interactions.

The structural motifs of the corresponding global optimization can be seen in Figure 3.20. Not much can be said from the energetics of the system, since on its own, there is nothing to compare it with.

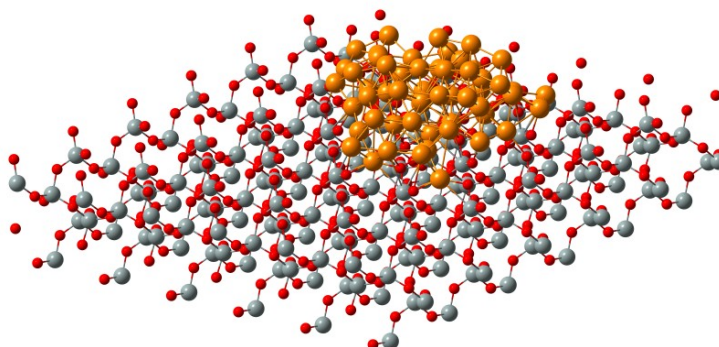


Figure 3.20: GA optimized  $\text{Cu}_{55}$  structure found on  $\text{SiO}_2(0001)$  surface, using the COMB2A potential.

### 3.5 Cu<sub>55</sub>-ZnO

Much more interesting than the two previous supported systems, is the ZnO(0001) supported Cu<sub>55</sub>. The shape of the optimized copper cluster on this surface allowed for a meaningful study of interface interactions. From the first GA optimization a semi-symmetrical cluster was formed on the zinc oxide substrate. Unlike the cases of TiO<sub>2</sub>, we observe limited wetting of the cluster over the surface, this will be shown later in Figure 3.22. This result replicates to some extent the epitaxial-only sort of interactions considered for the most cases of supported clusters on the literature. Next, the possibility of creating a mixed Cu/Zn/O interface was investigated. These GA searches were carried out by removing the surface atoms directly beneath the cluster and the bottom layer of cluster atoms. These atoms were then re-introduced to the system via the GA optimization. In this way, the GA search worked in a limited configurational space, delimited by the volume between the carved surface and the top part of the copper cluster. From this it was even possible to study oxidized ZnO and ZnO with oxygen vacancies. A schematic picture of this carved surface can be appreciated in Figure 3.21. The left side shows the lateral view, while the right side shows the top view. For the top view, all layers but the first were intentionally removed from the substrate to show the hole carved in the surface.

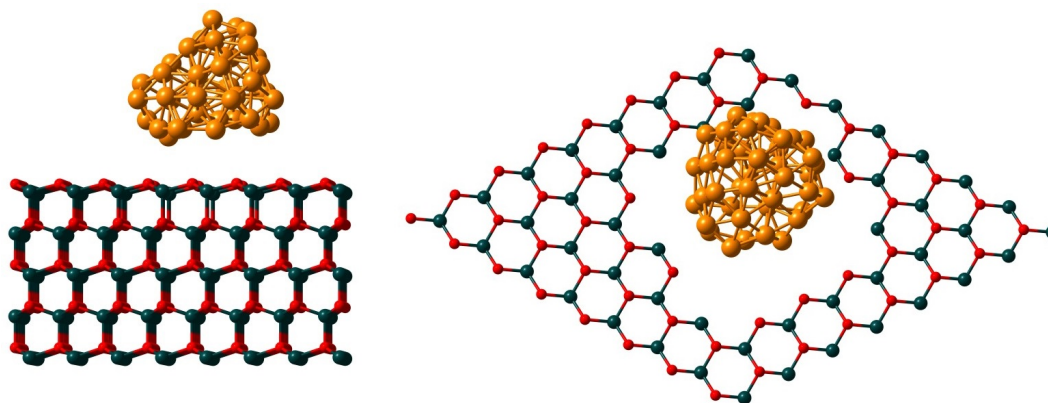


Figure 3.21: Schematic picture of carved surface.

#### 3.5.1 Neutral ZnO

##### Ideal surface

As it has been described for the other surfaces, the first GA optimization worked on the Cu<sub>55</sub> cluster. The same methodology and parameters described for the SiO<sub>2</sub> and TiO<sub>2</sub> were used. The structural motif obtained was the result of the first GA search, which consisted of twenty runs, with twenty candidates per run. The resulting structure from these GA searches can be seen in Figure 3.22.

A closer look at the supported cluster shows some (111) facets than can be also seen in the icosahedral Cu<sub>55</sub> gas-phase cluster. From this structure, we managed to

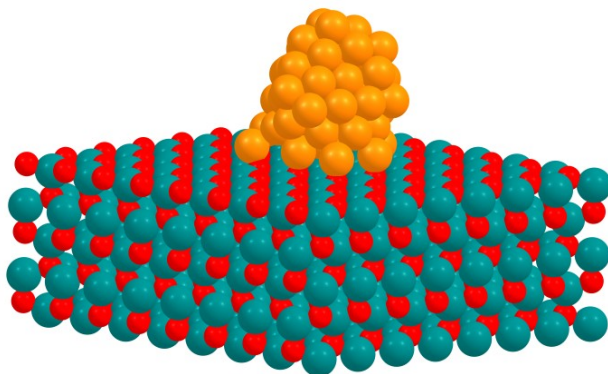


Figure 3.22: Lowest energy  $\text{Cu}_{55}$  structure supported on an ideal  $\text{ZnO}(0001)$  substrate.

create a "mixed interface" optimization, constructed as described before.

### Mixed interface

In the case of the mixed interface, a couple of changes were introduced to the GA optimization. Here, the permutation mutation was used as the main mutation operator. The selection probabilities were divided as 25% for the mirror mutation, 25% for the rattle mutation and 50% probability for the permutation mutation. On top of this, the overall mutation probability was increased to 40%, in order to help avoid any type of structural stagnation. The number of atoms optimized at the interface were 14 oxygen, 14 zinc and 12 copper. Two thousand iterations were conducted before finalizing the GA search.

The structural motif of the most stable structure found by the GA is presented in Figure 3.23. This figure shows a clear diffusion of zinc and oxygen atoms from the slab to the cluster. The same goes the other way around, with copper atoms taking positions on the surface. There does not seem to be any tendency of any atomic species clustering in a particular place.

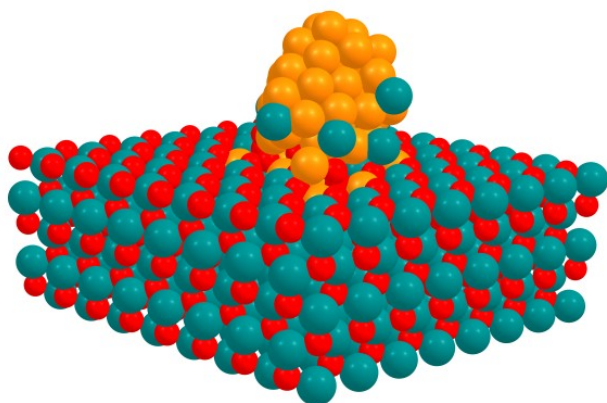


Figure 3.23: GM  $\text{Cu}_{55}$  supported on a mixed interface  $\text{ZnO}$  substrate.

The configurational differences are not only clearly visible between the two structures, but, according to the relaxations made with the COMB3 potential, the "*mixed interface*" structure is more energetically favorable by  $\sim 11$  eV. This can be appreciated in detail in Table 3.11

	<b>Ideal interface</b>	<b>Mixed interface</b>
$E_{\text{tot}}$ (eV)	-2430.218	-2441.068
$E_{\text{relative}}$ (eV)	0	-10.85

Table 3.11: Energetic differences of the lowest energy structure in the *ideal interface* vs. the *mixed interface* for neutral ZnO-Cu<sub>55</sub>.

In order to evaluate the accuracy of the COMB results, a set of DFT calculations were performed on these two structural motifs. These calculations were made with the CP2K software, using a combination of GTH pseudo-potentials coupled to LCAO double zeta basis set and the PBE exchange correlation potential to effectively evaluate the systems electronic density and total energy. Convergence was set to 50 meV/Å. More on this can be found in the second chapter. Also, two second-lowest energy structures (S.L.E.S.) were selected for each of these two cases as it is possible that the DFT global minimum lies closer to one of these structures. Energetical data is presented as follows.

For the stoichiometric surface-cluster (ideal) interface, the energies are shown in Table 3.12.

<b>Stoichiometric</b>	<b>Putative GM</b>	<b>S.L.E.S C1</b>	<b>S.L.E.S C2</b>
$E_{\text{tot}}$ (eV)	-738951.108	-738951.134	-738952.711
$E_{\text{relative}}$ (eV)	0	-0.026	-1.603

Table 3.12: Energies for stoichiometric (ideal) ZnO-Cu<sub>55</sub> from DFT calculations

While for the mixed interface, the results are shown in Table 3.13. Note that the reference for the  $E_{\text{relative}}$  is taken as the *putative GM* for the *stoichiometric* ideal interface DFT calculation.

<b>Mixed Interface</b>	<b>Putative GM</b>	<b>S.L.E.S C1</b>	<b>S.L.E.S C2</b>
$E_{\text{tot}}$ (eV)	-738934.379*	-738935.705**	-738942.045***
$E_{\text{relative}}$ (eV)	16.729*	15.403**	9.063***

Table 3.13: Energy for ZnO-Cu<sub>55</sub> mixed interface from DFT calculations

We must note that none of the calculations for the mixed interface are fully converged (\* 0.6695 eV/Å, \*\* 0.7556 eV/Å, \*\*\* 1.0683 eV/Å). Still, the smallest energy difference between the mixed and the ideal interfaces is  $\sim 10$  eV, in favour of the ideal stoichiometric interface. Even more, it must be noted that for both the mixed and ideal interfaces, one of the S.L.E.S. was actually a lower minimum structure.

As a result, one important conclusion is that the COMB parametrizations are not sufficiently accurate for this sort of systems.

### 3.5.2 Oxygen deficient ZnO - Cu<sub>55</sub>

Regardless of these previous results for the stoichiometric systems, it is interesting to consider the cases of oxidized and oxygen deficient surfaces. Due to time limitations, it was only possible to obtain the results for these systems under the GA+IP formalism. For these compositions, essentially the same GA methodology was used.

The oxygen deficient structures are interesting, since oxygen deficiencies on the surfaces mean vacancies that can be occupied by other atomic species. This sort of anchoring mechanism was mentioned before, when discussing the TiO<sub>2</sub> supported Cu<sub>55</sub> cluster.

#### 3.5.2.1 Ideal surface

In this case, two situations were considered for the "*ideal surface*", while a simple carved surface was made for the "*mixed interface*". These procedures have been discussed and described in the previous subsection. The two cases considered for the "*ideal surface*" correspond to whether it is preferable or not to have clustering of oxygen vacancies. In the "clustered" case, six vacancies were located directly below the copper cluster (C1). In the "diluted" case, 6 oxygen vacancies were created at the surface in a homogeneous way (C2). In the GA optimization, only the twelve bottom atoms from the ideal putative-GM considered in the previous subsection were optimized. All atoms on the substrate were fixed. Once again the GA search consisted of twenty runs, where each run had a population of twenty randomly generated initial candidates. Each GA run was iterated two thousand times. The permutation mutation was turned off for the ideal surfaces, and the probability of eligibility for the two remaining mutations was kept at 50-50. The energies for the diluted and clustered cases are shown in Table 3.14.

6O Deficient	Clustered (C1)	Dilute (C2)
E <sub>tot</sub> (eV)	-2400.023	-2399.890
E <sub>relative</sub> (eV)	0	0.133

Table 3.14: Energy comparison for oxygen deficient ZnO-Cu<sub>55</sub> from the ideal putative GM.

The energy difference is too small to really tell anything apart from these two. Given the accuracy of the COMB potential, it's fair to say that both cases are equally preferred energetically speaking. However, these two structures are significantly different, when considering structural motifs. The C1 structure (clustered vacancies), allows for copper atoms to embed themselves into the surface. While the C2 (diluted vacancies), only allows for epitaxial interaction between surface and

cluster. These differences can be seen in the Figures 3.24 and 3.25. These results still need to be validated by DFT calculations.

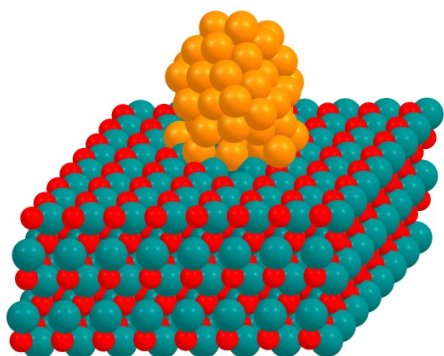


Figure 3.24: Oxygen deficient ZnO-Cu<sub>55</sub> "clustered" vacancies structure (C1).

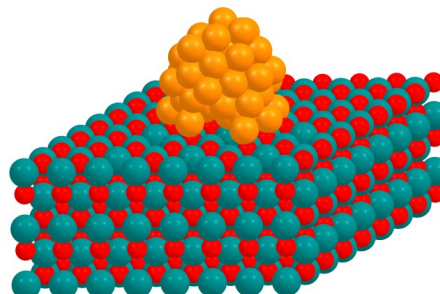


Figure 3.25: Oxygen deficient ZnO-Cu<sub>55</sub> "diluted" vacancies structure (C2).

### 3.5.2.2 Mixed interface

For the mixed interface in the oxygen deficient surface, the same procedure was followed as for the stoichiometric calculations, but 6 oxygen atoms were removed from the GA optimization. i.e, there were only eight oxygen atoms in the GA optimization, instead of the fourteen found in the stoichiometric case. In this case, the system's relative energy with respect to the ideal "diluted" oxygen deficient substrate (C1) was found to be lower by 11.874 eV. Once more, the preference in energy from the COMB calculations goes to the mixed interface structure, yet, this results must be taken with a pinch of salt. From Figure 3.26, we can see that copper atoms go to the first layer of the surface, while many zinc atoms seem to decorate the external border of the nanoparticle. This behaviour has not been seen in the other structures.

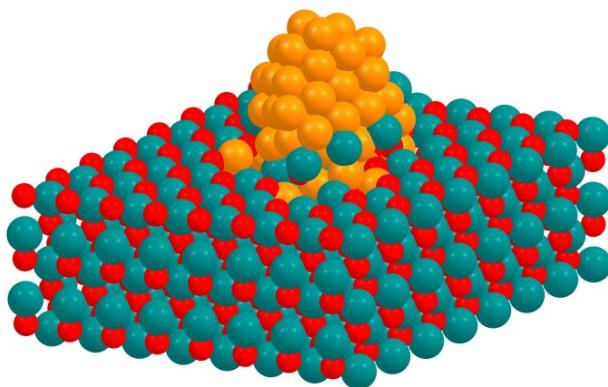


Figure 3.26: Lowest energy Cu<sub>55</sub> structure on the oxygen deficient mixed interface support.

### 3.5.3 Oxidized ZnO - Cu<sub>55</sub>

A similar procedure was done to check for the effect of excess oxygen in the structure. In the case of the ideal surface, six oxygen atoms were optimized via GA optimization along with the bottom twelve copper atoms. While in the case of the mixed interface, six extra oxygen atoms are included along with the regular fourteen zinc, fourteen oxygen and twelve coppers. The regular approach is then followed.

There is nothing special about the mixed surface structure, when it comes to geometrical motif, except maybe that more oxygen atoms can be seen at the interface between the bottom layer of copper atoms and the zinc oxide surface (See Figure 3.27). On the other hand, the ideal surface with additional oxygen atoms completely scrambles the bottom layer of copper atoms across the surface. This can be seen in the Figure 3.28. It remains to be seen whether this special behaviour persists when using more accurate descriptions of the PES. The ideal surface system energy is -2463.280 eV, compared to the -2471.241 eV for the mixed surface (7.961 eV lower). Further DFT calculations would be needed to really tell anything about the tendency towards interfacial mixing in both the O-rich and O-deficient cases, as well as the stoichiometric case.

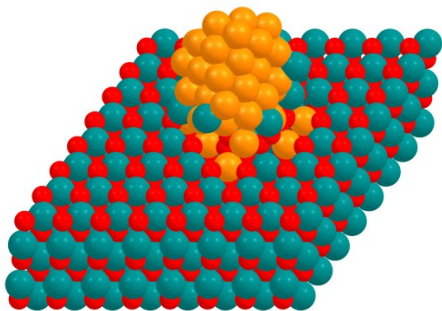


Figure 3.27: Lowest energy Cu<sub>55</sub> structure with oxygen excess on the mixed interface support.

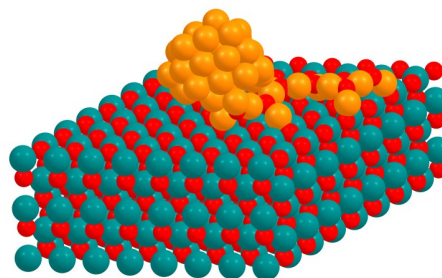


Figure 3.28: Lowest energy Cu<sub>55</sub> structure with oxygen excess on the ideal interface support.

# Conclusions

In this master thesis, a global optimization study of oxide-supported metallic nanoparticles was carried out.  $\text{Cu}_{55}$  supported on  $\alpha$ -quartz  $\text{SiO}_2(0001)$ , rutile  $\text{TiO}_2(110)$  and wurtzite  $\text{ZnO}(0001)$  substrates were used as model systems to investigate the preferred metal/oxide interface structure and conformation. The charge optimized many-body (COMB) potentials, coupled to genetic algorithm (GA) searches, were utilized to determine the structural motif of the supported nanoparticle. A second GA optimization was made to study the formation of mixed oxides between the particle and the support. Finally, the effect of oxygen vacancies and oxygen excess at the metal/oxide interface was investigated following the same framework as before. DFT re-optimization of the neutral  $\text{Cu}_{55}$ - $\text{ZnO}$  lower energy structures, for both the mixed and ideal interfaces, was performed. The computational framework necessary to carry out this thesis work was successfully adapted from the open-source ASE-GA code.

The results obtained from the first GA optimization for  $\text{Cu}_{55}$ - $\text{SiO}_2$  and  $\text{Cu}_{55}$ - $\text{TiO}_2$ , hindered the possibility of investigating interface interactions in such systems. For the specific case of the  $\text{TiO}_2(110)$  substrate, the lowest energy structure of  $\text{Cu}_{55}$  was found to be a complete monolayer. This structural motif for the copper particle was obtained with both versions the COMB potential. We believe that this result is a consequence of poor parametrization of the potential for Ti-O-Cu interactions. In the case of  $\text{Cu}_{55}$  on  $\text{SiO}_2(0001)$ , the lowest energy structure found after the GA optimization showed no icosahedral symmetry whatsoever. This lack of icosahedral symmetry lead us to believe that the nanoparticle structure was still far from the global minimum. Further optimization of this structure is needed if one wishes to investigate interface structure and conformation.

The lowest energy structure found from the first GA optimization for the  $\text{Cu}_{55}$  on  $\text{ZnO}(0001)$  allowed for further research on interface interactions. The optimized nanoparticle showed some remnant icosahedral symmetry with respect to its gas phase structure. Some (111) facets could also be appreciated in the GA optimized supported nanoparticle. From this, the GA optimization to study interface conformation with the COMB potential followed. The results obtained from the second GA optimization showed that atom exchange between surface and nanoparticle at the interface was preferred over the simple epitaxial interaction of the pristine neutral structure.

The effect of oxygen vacancies and oxygen excess at the metal/oxide interface was investigated with GA optimization still making use of the COMB potentials. The oxygen vacancies study showed that mixing at the interface was a energetically more favorable interaction than the pristine interface interaction. Out of the two

tested cases for the pristine interface, the "Clustered" vacancies seemed to anchor the nanoparticle in the surface, in a very real sense, the nanoparticle was embedded into the surface. For the mixed interface, zinc atoms seemed to decorate the perimeter of the NP, while, for the most part, oxygen atoms remained at the interface between the NP and the substrate. For the oxidized interface structure, we saw the same trend as for the neutral stoichiometric and the oxygen deficient cases. Mixing of the interface was preferred over the pristine oxide-nanoparticle interface. The results obtained here for the pristine interface case were somewhat special, the interfacial copper atoms were smeared over the surface, situation observed here for the first time in this study. In the case of the mixed surface, similarly as for the oxygen deficient case, the zinc atoms decorated the perimeter of the nanoparticle.

DFT re-optimization of the three lower energy structures obtained from the first GA searches were made for the neutral stoichiometric case of study. The results obtained from these first principles calculations pointed towards a different conclusion than what the COMB results seemed to imply. The DFT optimizations showed that, for the structures obtained from the first GA optimization, the pristine oxide-nanoparticle interface was energetically favorable over the mixed interface. On top of this, the lowest energy structure founded with the COMB potential turned out to be a higher standing minimum compared to second lowest energy structures (SLES) after DFT optimization. For both the mixed and the pristine interfaces at least one of the SLES had lower energy than the correspondent putative IP-GM. These results suggested that the COMB potentials tend to overestimate the energy for the mixed interface system. DFT optimization of the oxidized and oxygen deficient ZnO-Cu<sub>55</sub> structures are still needed to determine unequivocally the effect oxygen vacancies and oxidation have on the interface interaction and conformation.

We conclude this thesis work by stating that genetic algorithms are efficient computational tools to make global optimization studies of supported nanometric particles. Also, and most importantly, we conclude that the COMB interatomic potential is not accurate enough to fully determine the behaviour of interactions at the interface of oxide supported metal nanoparticles. This conclusion is based on the results obtained from the DFT re-optimization of the neutral Cu<sub>55</sub>-ZnO structures. As a final remark, although computationally expensive, first principles global optimization studies are necessary to elucidate with certainty if there is any mixing of atoms at the interface in these systems.

# Bibliography

- [1] Dresselhaus, M.S.; Thomas, I.L.(2001). *Nature*, 414, 332.
- [2] Johnston, R.L. (2002). *Atomic and Molecular Clusters*. 1st Ed. Master Series in Physics and Astronomy. (D.S. Betts(Eds.)). Suffolk:St Edmundsbury Press.
- [3] Johnston,R.L.(2012).*Metal Nanoparticles and Nanoalloys*.(pp 1-38). 1st ed, Vol.3, Frontiers of Nanoscience.(J. Wilcoxon & R.L. Johnston (Eds.)). Oxford, UK: Elsevier.
- [4] Mariscal, M.M.; Oviedo, O. A.; Leiva, E. P. M. (2013).[Preface]. *Metal Clusters and Nanoalloys: From Modeling to Applications*. (pp v-vi). 1st ed. Nanostructure Science and Technology.(Mariscal, M.M.; Oviedo, O. A.; Leiva, E. P. M. (Eds.)). New York: Springer.
- [5] Roldan Cuenya, B. (2015). Nanocatalysis: Size- and shape-dependet chemisorption and catalytic reactivity. *Surface Science Report*, 70, 135-187.
- [6] Chorkendorff, I.; Niemantsverdriet, W. (2003) *Concepts of Modern Catalysis and Kinetics*. 1st ed. Weinheim: Willey-VCH.
- [7] Bussaca, C. *et al.* (2011).The growing impact of catalysis in the pharmaceutical industry.*Adv. Synth. Catal.*353, 1825-1864.
- [8] van Santen, R.A. & Niemantsverdriet, J.W. (1995). *Chemical Kinetics and Catalysis*. 1st ed. Fundamental and applied catalysis. (M.V. Twigg & M.S. Spencer (Eds.)). New York: Springer Science+Bussiness Media.
- [9] Freund, H.J & Ertl, G. (1999). Catalysis and Surface Science. *Physics Today*. Vol.52(1), 32-38.
- [10] Campbell, C.T. (2012). Catalyst-support interactions: Electronic Perturbations. *Nature Chemistry*, Vol. 4, 597-598.
- [11] de Jongh, P.E. *et al.* (2013). Towards stable catalysts by controlling collective properties of supported metal nanoparticles. *Nature materials*. Vol.12. 34-39.

- [12] Fortunelli, A. and Barcaro, G. (2013). *Metal Clusters and Nanoalloys: From Modeling to Applications*.(pp 29-80).1 st ed. Nanostructure Science and Technology. (Mariscal, M.M.; Oviedo, O. A.; Leiva, E. P. M. (Eds.)) New York: Springer.
- [13] Topsøe, H. (2003). Developments in operando studies and in situ characterization of heterogeneous catalysts. *Journal of Catalysis*, Vol.216, 155–164.
- [14] Mejia-Rosales, S. and Jose-Yacaman, M. (2013). *Metal Clusters and Nanoalloys: From Modeling to Applications*.(pp 3-28).1 st ed. Nanostructure Science and Technology. (Mariscal, M.M.; Oviedo, O. A.; Leiva, E. P. M. (Eds.)) New York: Springer.
- [15] Libuda, J. and Freund, H.J.(2005). Molecular beam experiments on model catalysts. *Surface Science Reports*, Vol.57, 157-298.
- [16] Somorjai, G.A. and Li, Y. (2010). Nanoscale Advances in Catalysis and Energy Applications. *Nano Lett*, vol.10, 2289-2295.
- [17] Cunningham A. and Bürgi, T. (2013). *Amorphous Nanophotics*. (pp 1-38). 1st Ed. Nano-Optics and Nanophotics. (C. Rocksuhl and T.Scharf (Eds.)). Berlin: Springer.
- [18] Cui, Z.(2008). *Nanofabrication: Principles, Capabilities and Limits*. 1st Ed. New York: Springer.
- [19] Brueck, S.R.J. *et al.*. (2011). Nanostructured and Functional Materials Fabricated by Interferometric Lithography. *Advanced Materials*. Vol. 23, 147-179.
- [20] Cramer, C.J. and Truhlar, D.G .(2009). Density functional theory for transition metals and transition metal chemistry. *Phys.Chem.Chem.Phys*. Vol 11. 10757-10816.
- [21] Fortunelli, A. and Ferrando, R.(2012).*Metal Nanoparticles and Nanoalloys*.(pp 159-205). 1st ed, Vol.3, Frontiers of Nanoscience.(J. Wilcoxon & R.L. Johnston (Eds.)). Oxford, UK: Elsevier.
- [22] Heiles, S. and Johnston, R.L. (2013). Global Optimization of Clusters Using Electronic Structure Methods. *International Journal of Quantum Chemistry*, Vol.113, 2091–2109.
- [23] Levchenko, S.V.(2012).  $Au_N$  clusters ( $N=1-6$ ) supported on MgO(100) surfaces: Effect of exact exchange and dispersion interactions on adhesion energies. *Physical Review B*, Vol.85,155409.

- [24] Roldan Cuenya, B.(2010). Synthesis and catalytic properties of metal nanoparticles: Size, shape, support, composition, and oxidation state effects. *Thin Solid Films*, 518, 3127-3150.
- [25] Pestryakov, A.N. *et al.*.(2004) Study of copper nanoparticles formation on supports of different nature by UV-visible diffuse reflectance spectroscopy. *Chemical Physics Letters*, 385, 173-176.
- [26] Luches, P. and D'Addato, S. (2016). *Oxide Materials at Two-Dimensional Limit.*(pp 119-142). 1st Ed, Vol. 234. Springer Series in Material Science.(F.P. Netzer and A. Fortunelli (Eds.)). Switzerland: Springer Nature.
- [27] Diebold, U. *et al.*(2005). Growth of copper on single crystalline ZnO: surface study of a model catalyst. *Topics in Catalysis*. Vol.36, Nos. 1-4.
- [28] Watanabe, T. *et al.* (1995). Development of copper/zinc oxide-based multicomponent catalysts for methanol synthesis from carbon dioxide and hydrogen. *Applied Catalysis A: General*. Vol. 138, 311-318.
- [29] Wöll, C. (2007). The chemistry and physics of zinc oxide surfaces. *Progress in Surface Science*. Vol.82, 55-120.
- [30] Natesakhawat, S. *et al.*(2012). Active Sites and structure-Activity Relationships of Copper-Based Catalysts for Carbon Dioxide Hydrogenation to Methanol. *ACS Catalysis*. Vol. 2, 1667-1676.
- [31] Hansen, P.L. *et al.*(2002). Atom-Resolved Imaging of Dynamic Shape Changes in Supported Copper Nanocrystals. *Science*, Vol.295,5562, 2053-2055.
- [32] Huang, Z. *et al.* (2008). Highly Dispersed Silica-Supported Copper Nanoparticles Prepared by Precipitation-Gel Method: A Simple but Efficient and Stable Catalyst for Glycerol Hydrogenolysis. *Chem. Mater*. Vol.20, 5090-5099.
- [33] Zhang, X. *et al.* (2013). Mesoporous silica-supported copper-catalysts for homocoupling reaction of terminal alkynes at room-temperature. *New J. Chem.*, Vol.37, 1343.
- [34] Zhang, Y.Q. *et al.* (2012). Homo-coupling of terminal alkynes on a noble metal surface. *Nat. Commun*. Vol.3:1286. [doi: 10.1038/ncomms2291].
- [35] Cai, C. and He, Y. (2012). Terminal alkyne homocoupling reactions catalyzed by an efficient and recyclable polymer-supported copper catalyst at room temperature under solvent-free conditions. *Catal. Sci. Technol.*. Vol.2, 1126-1129.
- [36] Chen, C.S. (2012). Effect of Ti<sup>3+</sup> on TiO<sub>2</sub>-Supported Cu Catalysts Used for CO Oxidation. *Langmuir*. Vol.28, 9996-10006.[dx.doi.org/10.1021/la301684h].

- [37] Ding, K., Li, J., Zhang, Y. (2005). Cu and NO coadsorption on TiO<sub>2</sub>(110) surface: a density functional theory study. *THEOCHEM*. 728, 123-127.
- [38] Rodriguez, J.A. *et al.* (2009). High Water-Gas Shift Activity in TiO<sub>2</sub>(110) Supported Cu and Au Nanoparticles: Role of the Oxide and Metal Particle Size. *J. Phys. Chem. C*, Vol.113, No.17.
- [39] Rodriguez, J.A. *et al.* (2014). Highly active copper-ceria and copper-ceria-titania catalysts for methanol synthesis from CO<sub>2</sub>. *Science*, Vol.345, 546-550. [doi: 10.1126/science.1253057]
- [40] Wales, D.J.(2003). *Energy Landscapes with Applications to Clusters, Biomolecules and Glasses*. 1st Ed. UK: Cambridge University Press.
- [41] Lewars, E.G.(2010). *Computational Chemistry: Introduction to the Theory and Applications of Molecular and Quantum Mechanics*. 2nd Ed. :Springer.
- [42] Leach, A.R. (2001). *Molecular Modelling: Principles and Applications*. 2nd Ed. England: Pearson Education Limited.
- [43] Szabo, A. and Ostlund, N.S. (1996). *Modern Quantum Chemistry: Introduction to Advanced Electronic Structure*. 1st Ed. New York: Dover Publications, Inc.
- [44] Miller, M.A, Doye, J.P.K and Wales, D.J. (1999). Structural relaxation in Morse clusters: Energy landscapes. *The Journal of Chemical Physics*, Vol.110, 328. [doi: 10.1063/1.478067]
- [45] Hohenberg, P. and Kohn, W. (1964). Inhomogeneous electron gas. *Phys.Rev.* Vol.136, A1441.
- [46] Kohn, W. and Sham, L.J. (1965). Self-consistent equations including exchange and correlation effects. *Phys.Rev.* Vol.140, 2264.
- [47] Vilhelmsen, B.L. and Hammer, B. (2014). A genetic algorithm for first principles global structure optimization of supported nano structures. *The Journal of Chemical Physics*. Vol.141, 044711. [doi: 10.1063/1.488633].
- [48] Ferrando, R., Jellinek, J., Johnston, R.L. (2008). Nanoalloys: From Theory to Applications of Alloy Clusters and Nanoparticles. *Chem. Rev.* Vol.108, (3), pp 845–910.
- [49] Barcaro, G., Aprà, E. and Fortunelli, A. (2007). Structure of Ag Clusters Grown on Fs-Defect Sites of an MgO(100) Surface. *Chem. Eur. J.* Vol.13, 6408–641.

- [50] Liang, T. *et al.* (2013). Classical atomistic simulations of surface and heterogeneous interfaces with the charge-optimized many body (COMB) potentials. *Materials Science and Engineering R*, Vol.74, 255-279.
- [51] Paz Borbon, L.O. (2011). *Computational Studies of Transition Metal Nanoalloys*. Springer Theses. Berlin: Springer.
- [52] Pauling, L. (1947). Atomic Radii and Interatomic Distances in Metals. *J. Am. Chem. Soc.* Vol. 69, 3, 542-553. DOI:10.1021/ja01195a02
- [53] Abell, G.C. (1985). Empirical chemical pseudopotential theory of molecular and metallic bonding. *Physical Review B*, Vol.31, 10, 6184–6196.
- [54] Brenner, D. W. (2000). The Art and Science of an Analytic Potential. *phys. stat. sol. (b)*, Vol.217, 23.
- [55] Tersoff, J. (1988). New empirical approach for the structure and energy of covalent systems. *Physical Review B*. Vol.37, 12, 6691-7000.
- [56] Mottet, C. *et al.* (2004). Modeling free and supported metallic nanoclusters: structure and dynamics, *Phase Transitions*, 77:1-2, 101-113.
- [57] Ferrando, R. *et al.* (2009). Structures of metal nanoparticles adsorbed on MgO(001). I. Ag and Au . *The Journal of Chemical Physics*, Vol.130, 174702.
- [58] Rappè, A.K and Goddard, A III. (1991). Charge Equilibration for Molecular Dynamics Simulations. *J. Phys. Chem.* Vol. 95, 3358-3363.
- [59] Mortier, W.J. *et al.* (1985). Electronegativity Equalization: Application and Parametrization. *J. Am. Chem. Soc.*, Vol.107,4, 829-835.
- [60] Cheng, Y-T. (2013). *Reactive variable charge potential development and atomistic simulations of surface and heterogeneous interfacial interactions*. (Doctoral dissertation). Retrieved from: University of Florida Digital Collections (<http://ufdc.ufl.edu/UFE0046194/00001>).
- [61] Liang, T. *et al.*. (2012). Variable Charge Reactive Potential for Hydrocarbons to Simulate Organic-Copper Interactions. *J.Phys.Chem.A* Vol.116, 7976-7991. [dx.doi.org/10.1021/jp212083t](http://dx.doi.org/10.1021/jp212083t)
- [62] Shan, T, *et al.*. (2011). Molecular dynamics study of the adhesion of Cu/SiO<sub>2</sub> interfaces using a variable-charge interatomic potential *Physical Review B*. Vol.83, 115327.
- [63] Wales, D.J. and Bogdan, T.V. (2006). Potential Energy and Free Energy Landscapes. *Phys. Chem. B*. Vol.110, 20765-20776.

- [64] Kirkpatrick, S.; Gellatm C.D.; Vecchi, M.P. (1983). Optimization by simulated annealing. *Science*. Vol.220, 4598.
- [65] Goedecke, S. (2004). Minima hopping: An efficient search method for the global minimum of the potential energy surface of complex molecular systems. *The Journal of Chemical Physics*, Vol.120, 9911; doi: 10.1063/1.1724816.
- [66] Wales, D.J. and Doye, J.P.K. (1997). Global Optimization by Basin-Hopping and the Lowest Energy Structures of Lennard-Jones Clusters Containing up to 110 Atoms. *J.Phys.Chem.A.*, Vol.101, 28, 5111-5116
- [67] Johnston, R.L. (2003). Evolving better nanoparticles: Genetic algorithms for optimising cluster geometries. *Dalton Trans.*, 2003, 4193-4207.
- [68] Chua, A.L.-S. *et al* .(2010). A genetic algorithm for predicting the structures of interfaces in multicomponent systems. *Nature Materials*, Vol.9. DOI:10.1038/NMAT2712.
- [69] Oganov A.R., Glass C.W. (2006). Crystal structure prediction using evolutionary algorithms: principles and applications. *J. Chem. Phys.* Vol.124, 244704.
- [70] Lonie, D.C. and Eva Zurek, E.(2011). XtalOpt: An open-source evolutionary algorithm for crystal structure prediction. *Computer Physics Communications*. Vol.182, 372–387.
- [71] Vilhelmsen, L.B and Hammer, B. (2012). Systematic Study of Au<sub>6</sub> to Au<sub>12</sub> Gold Clusters on MgO(100) F Centers Using Density-Functional Theory. *Physical Review Letters*, Vol.108, 126101. DOI:10.1103/PhysRevLett.108.126101.
- [72] Module standardmutations. (n.d.). Retrieved June 1st, 2016, from <https://wiki.fysik.dtu.dk/ase/epydoc/ase.ga.standardmutations-module.html>.
- [73] Yufei, Z. *et al*. (2010). First principles of Wurtzite ZnO (0001) and (000-1) surface structures. *Journal of Semiconductors*, Vol. 31, Issue 8.
- [74] Karzel H. *et al*. (1996). Lattice dynamics and hyperfine interactions in ZnO and ZnSe at high external pressures. *Phys Rev B*, Vol.53, No.17, 11425-11438.
- [75] Keskar, N.R and Chelikowsky, J.R. (1992). Structural properties of nine silica polyphorms. *Physical Review B*, Vol.46, No.1.
- [76] Levien, L. *et al*. (1980). Structure and elastic properties of quartz at pressure. *American Mineralogist*, Vol.65, 920-930

- [77] Montanari, B. and Harrison, N.M. (2002). Lattice dynamics of TiO<sub>2</sub> rutile: influence of gradient corrections in density functional calculations. *Chemical Physics Letters*, Vol.364, Issues 5–6, 528–534.
- [78] Burdett, J.K. *et al.* (1987). Structural-electronic relationships in inorganic solids: powder neutron diffraction studies of the rutile and anatase polymorphs of titanium dioxide at 15 and 295 K. *Am. Chem. Soc.*, Vol.109, No.12, 3639–3646.
- [79] Singh, T; Mountziaris, T.J. and Maroudas, D. (2010). On the transition-metal doping efficiency of zinc oxide nanocrystals. *Applied Physics Letters*, Vol.97, 073120. doi: 10.1063/1.3478216.
- [80] Goumans, T.P.M *et al.* (2007). Structure and stability of the (001)  $\alpha$ -quartz surface. *Phys. Chem. Chem. Phys.*, Vol.9, 2146-2152. DOI: 10.1039/B701176H.
- [81] Fox, H. *et al.* (2010). Bulk and Surface Properties of Rutile TiO<sub>2</sub> from Self-Consistent-Charge Density Functional Tight Binding. *J. Chem. Theory Comput.* Vol.6, 499–507.
- [82] Lazzeri, M. ; Vittadini, A. and Selloni, A. (2001). Structure and energetics of stoichiometric TiO<sub>2</sub> anatase surfaces. *Physical Review B*, Vol.63, 155409.
- [83] Cheng, Y-T. *et al.* (2014). A charge optimized many-body (comb) potential for titanium and titania. *J. Phys.: Condens. Matter.* Vol.26, 315007.
- [84] Darby, S. *et al.* (2002). Theoretical study of Cu–Au nanoalloy clusters using a genetic algorithm. *The Journal of Chemical Physics.* Vol.116, 1536; doi: 10.1063/1.1429658
- [85] Rapps, T. *et al.* (2013). On the Structures of 55-Atom Transition-Metal Clusters and Their Relationship to the Crystalline Bulk. *Angew. Chem. Int.* Vol.52, 6102 –6105.
- [86] Deaven, D.M. and Ho, K.M. (1995). Molecular Geometry Optimization with a Genetic Algorithm. *Physical Review Letters*, Vol.75, No.2.
- [87] Barcaro, G. and Fortunelli, A. (2005). The Interaction of Coinage Metal Clusters with the MgO(100) Surface. *J. Chem. Theory Comput.* Vol.1, No.5, 972-985.